Deglacial to Holocene history of ice-sheet retreat and bottom current strength on the western Barents Sea shelf

Hendrik Lantzsch[1,2,*], Till J.J. Hanebuth[1,3], Jan Horry[2], Marina Grave[2], Michele Rebesco[4], Tilmann Schwenk[1,2]

[1] MARUM – Center for Marine Environmental Sciences, University of Bremen, Bremen, Germany.

[2] Faculty of Geosciences, University of Bremen, Bremen, Germany.

[3] School of Coastal and Marine Systems Science, Coastal Carolina University, Conway, SC, U.S.A.

[4] OGS – Istituto Nazionale di Oceanografia e di Geofisica Sperimentale, Sgonico, Trieste Italy.

* Corresponding author: Phone: + 49 421 218 65193; Fax: + 49 421 218 65219; E-mail: lantzsch@uni-bremen.de (H. Lantzsch).

Abstract

High-resolution sediment echosounder data combined with radiocarbon-dated sediment cores allowed us to reconstruct the Late Quaternary stratigraphic architecture of the Kveithola Trough and surrounding Spitsbergenbanken. The deposits display the successive deglacial retreat of the Svalbard-Barents Sea Ice Sheet. Basal subglacial till indicates that the grounded ice sheet covered both bank and trough during the Late Weichselian. A glaciomarine blanket inside the trough coinciding with laminated plumites on the bank formed during the initial ice-melting phase from at least 16.1 to 13.5 cal ka BP in close proximity to the ice margin. After the establishment of open-marine conditions at around 13.5 cal ka BP, a sediment drift was deposited inside the Kveithola Trough, contemporary with a crudely laminated mud, an overlying lag deposit, and modern bioclastic-rich sand on Spitsbergenbanken. The Kveithola Drift shows a remarkable grain-size coarsening from the moat towards the southern flank of the trough. This trend contradicts the concept of a separated drift and indicates that the southern bank is the main sediment source for the coarse material building up the Kveithola Drift. This depocenter represents, therefore, a yet undescribed combination of off-bank wedge and confined drift. Although the deposits inside

Kveithola Trough and on Spitsbergenbanken display different depocenter geometries, time-equivalent grain-size changes imply a region-wide sediment-dynamic connection. We thus relate a phase of coarsest sediment supply (8.8 to 6.3 cal ka BP) to an increase in bottom current strength, which might be related to a strong Atlantic Water inflow from the Southeast across the bank, which led to winnowing and off-bank export of sandy sediments.

Keywords

Contourite drift; Glacial trough; Bottom currents; Atlantic Water; Brine-enriched shelf water; Meltwater plumes; Kveithola; Spitsbergenbanken; Barents Sea; Late Quaternary

Highlights

- Lithological correlation of glacial trough and surrounding bank deposits
- Initial ice-melting in study area occurred earlier than 16.1 cal ka BP
- Establishment of open-marine conditions at around 13.5 cal ka BP
- Region-wide grain-size coarsening at 8.8 cal ka BP by strong bottom currents
- Remarkable lateral coarsening of the drift with increasing distance from the moat

1. Introduction

The deglacial changes of oceanographic configurations and sediment dynamics on polar continental shelves are a matter of debate due to the potential interplay of a wide variety of climatic, oceanographic, and environmental forcing mechanisms. In case the ice reservoir of an ice-stream system and the associated catchment area are of local extent, the deposits that typically form in such an environment may sensitively record deglacial changes (Rebesco et al., 2011; Hanebuth et al., 2013; Bjarnadóttir et al., 2013, 2014). Such a recorder is the Kveithola area, located in the NW Barents Sea, which hosts a trough that formed by isolated small-scale ice-stream carving and trapped sediment during and after ice coverage (Rebesco et al., 2011).

So far, the majority of sedimentary studies in the Kveithola area concentrated on deposits inside the trough (e.g., Rüther et al., 2012; Bjarnadóttir et al., 2013, 2014; Rebesco et al., 2011, 2016a) and on the continental slope (e.g., Blaume, 1992; Lucchi et al., 2012, 2013; Rebesco et al., 2014a; Llopart et al., 2014, 2015). This focus is the result of the coarse-grained nature of deposits on the surrounding Spitsbergenbanken. The few studies on Spitsbergenbanken almost entirely relied on surface samples (e.g., Edwards, 1975; Bjørlykke et al., 1978; Vorren and Laberg, 1996; Henrich et al., 1997; Elverhøi and Henrich, 2002). The Late Quaternary history of Spitsbergenbanken thus remains scarcely known. In order to unravel a comprehensive picture of the deglacial sedimentary evolution of the Kveithola area it is crucial to develop an area-wide stratigraphic correlation, linking the deposits of Kveithola Trough and surrounding Spitsbergenbanken in order to reveal information about the environmental forces controlling trough and bank depocenters, and to identify their specific sediment sources.

Within the Kveithola Trough, a shallow-water contourite drift forms the youngest and geographically well-confined depocenter (Rüther et al., 2012; Bjarnadóttir et al., 2013; Rebesco et al., 2016a). In contrast to deep-sea bottom currents forming contourite drifts *sensu stricto,* shallow-water bottom currents derive from a variety of processes such as thermohaline contour currents, cascading currents, wind-driven currents, and internal waves/tides (Verdicchio and Trincardi, 2008a). Hence, short-term changes in intensity and direction, eddies, and reverse flows may occur (Johnson and Baldwin, 1996). Nevertheless, shallow-water drift deposits exhibit a high lateral continuity, very limited hiatuses, and high accumulation rates, which makes them excellent environment-sensitive paleoceanographic archives (Rebesco and Camerlenghi, 2008; Rebesco et al., 2014b).

Some of the few examples of well-studied shallow-water contourite systems include the Campos Basin offshore southeast Brazil (Viana and Faugères, 1998; Viana, 2001), the southwestern Adriatic Margin (Cattaneo et al., 2003; Verdicchio and Trincardi, 2006), and the Eastern Gela Basin offshore southwestern Sicily (Verdicchio and Trincardi, 2008b). Hence, very few comprehensive studies were carried out and the interplay of controlling processes remains poorly understood. The sediment-acoustic facies of the Kveithola Drift was studied by various authors (Rüther et al., 2012; Bjarnadóttir et al., 2013; Rebesco et al., 2016a). However, the description of the sedimentary system was rather general and the factors controlling the spatial and temporal evolution of this depocenter as well as the specific sediment sources remained speculative.

With consideration of these gaps in knowledge, we present new data from Kveithola Trough and Spitsbergenbanken including a grid of sediment-echosounder profiles and dated sediment cores. The aim of this study was to: (1) reconstruct the Late Quaternary architectural development and temporal relationship of both Kveithola Trough and Spitsbergenbanken sedimentary successions; and (2) reveal sediment sources and local sediment distribution mechanisms in order to improve the shallow-water contourite concept.

2. Regional settings

The NW margin of the Barents Sea shelf is dissected by E-W trending glacially carved morphological troughs such as Storfjorden Trough and Bear Island Trough. The Kveithola Trough is located between these two larger features and extends over 90 km at widths of less than 15 km and water depths between 300 to 350 m along its axis (Fig. 1). The U-shaped cross profile and the presence of mega-scale glacial lineations (MSGL; cf. Stokes and Clark, 1999) indicate that a fast-flowing ice stream shaped this trough emerging from the Svalbard-Barents Sea Ice Sheet (SBIS; Vorren and Laberg, 1996; Andreassen et al., 2008; Rebesco et al., 2011; Bjarnadóttir et al., 2013, 2014). The MSGL are overprinted by transverse grounding-zone wedges (GZWs; cf. Dowdeswell et al., 2008) formed by ice-grounding events punctuating the rapid deglacial ice sheet retreat (Rebesco et al., 2011; Bjarnadóttir et al., 2013). A 15 to 40-m thick glaciomarine sediment drape caps the GZWs and is composed of material generated by ice rafting and meltwater plumes (Rebesco et al., 2011; Bjarnadóttir et al., 2013; Lucchi et al., 2013; Hanebuth et al., 2014). This glaciomarine blanket formed during the Bølling-Allerød interval (Rüther et al., 2012; Bjarnadóttir et al., 2013). The youngest unit represents a sediment drift that occupies the inner part of the Kveithola Trough (Fig. 1; Rüther et al., 2012; Bjarnadóttir et al., 2013; Rebesco et al., 2016a). According to Rüther et al. (2012), the Kveithola sediment drift formed after 13.1 cal ka BP. A channel intersecting the northern flank of the inner Kveithola Trough was suggested to be the main conduit for cascading dense-water bottom currents supplying sediment to the Kveithola Drift complex (Fig. 1; Fohrmann, 1996; Fohrmann et al., 1998; Bjarnadóttir et al., 2013, Rebesco et al., 2016a).

The Kveithola Trough is surrounded by Spitsbergenbanken (Fig. 1), a geographic region that extends between Bear Island and Hopen Island. Including wide areas above 30 m water depth, Spitsbergenbanken is the shallowest bank in the Barents Sea. The modern depositional environment was described as the largest Arctic cold-water carbonate platform (Henrich et al., 1997). A kelp forest occupies the central part of the bank in water depths of less than 25 m, flanked by high-energy bioclastic carbonate sands and mollusk/glaciomarine-gravel lag deposits (Bjorlykke et al., 1978; Henrich et al., 1997). During the Late Weichselian, Spitsbergenbanken was covered by the SBIS resulting in extended till deposition (Elverhøi and Henrich, 2002). According to Landvik et al. (1998), Ślubowska-Woldengen et al. (2008), and Jessen et al. (2010), shallow Spitsbergenbanken was still covered by the SBIS during Bølling-Allerød times (14.5 to 13.5 cal ka BP). Deglacial retreat of the SBIS is shown by the deposition of a diamicton with rare molluskan infauna (Elverhøi and Henrich, 2002). A gravel lag and carbonate-rich sands that deposited in a glaciomarine environment cap this diamicton on Spitsbergenbanken (Elverhøi and Henrich, 2002).

Two main water masses determine the present oceanographic situation in the study area, Atlantic Water and Arctic Water (Fig. 1). The warm Atlantic Water flows northward along the continental slope as West Spitsbergen Current, a branch of the Norwegian Atlantic Current (Swift, 1986). Atlantic Water intrudes eastward where the Barents Sea continental shelf is dissected by troughs (Fig. 1). The earliest inflow of Atlantic Water to the Nordic Seas started at 16 to 15 cal ka BP, and relatively strong inflow was described for Bølling-Allerød and early Holocene (Ślubowska-Woldengen et al., 2008; Carbonara et al., 2016; Bøe et al., 2017; Rigual-Hernández et al., 2017). The cold and less saline Arctic Water enters the NW Barents Sea as East Spitsbergen Current from the north and occupies large parts of the Barents Sea (Fig. 1; Loeng, 1991). Spitsbergenbanken Water represents a mixture of Arctic Water and summer meltwater but is restricted to central parts of Spitsbergenbanken.

3. Materials and Methods

3.1 Acoustic profiling and sediment coring

Sediment-acoustic data were collected by means of the parametric sediment echosounder ParaSound P70 (Teledyne Reson) during Cruise MSM30 CORIBAR ("Ice dynamics and meltwater deposits: coring in the Kveithola Trough, NW Barents Sea") with the German research vessel MARIA S. MERIAN in 2013 (Fig. 1; Hanebuth et al., 2013). The primary high and low frequencies of the system were set to 18 and 22 kHz, respectively, leading to a secondary parametric signal of 4 kHz for sub-bottom profiling, which enables a vertical resolution on decimeter scale. Two hull-mounted echosounder systems were used for bathymetric mapping, a Kongsberg Simrad EM 122 in deeper waters, and an EM 1002 in shallower waters.

The GeoB sediment cores were collected during the same cruise (Fig. 1; Table 1; Hanbebuth et al., 2013). A vibrocorer and a gravity corer were used to recover sandy and muddy sediments, respectively. In addition, a multicorer and a giant box corer were deployed to sample the undisturbed modern sediment surface.

3.2 Lab analyses

Detailed visual description was performed for each sediment core. In order to validate the visual core descriptions and the determination of facies types, 1-cm thick radiography slabs were taken from selected intervals.

On sediment cores from the trough, the grain-size distribution from 2000 to 0.4 µm was analyzed with a Coulter Laser Particle Sizer LS200. In order to isolate the terrigenous fraction prior to analysis, each sample was treated in successive steps with 35% H2O2, 10% HCl, and 6% NaOH to remove organic carbon, biogenic carbonate, and opal, respectively. Sediment samples from the bank often contain larger amounts of sand and gravel at grain sizes, which are at the upper measurement limit. Therefore, the coarse fraction (> 63 µm) was separated from the fine fraction (< 63 µm) by wet sieving as a first step. The coarse fraction was then sonic-sifted into grain-size subfractions. Grain-size spectra of the terrigenous fine fraction were quantitatively analyzed by a Micromeritics Sedigraph with an effective range of 0.1 to 300 µm. Measurements of the fine fraction were forewent if the samples contained predominantly (i.e. > 50 %) sand and gravel. We are aware that a precise quantitative comparison of grain-size measurements from Coulter Laser Particle Sizer and Micromeritics Sedigraph cannot be done due to different methodological approaches. In the instances where grain sizes of bank and trough sediments are directly compared with each other, we concentrate on general trends rather than using this data for a quantitative consideration.

Total carbon (TC) and total organic carbon (TOC) contents were quantified using a LECO CS-200 system. Calcium carbonate contents were calculated by the standard equation $CaCO_3$ [weight %] = (TC - TOC) 8.333. X-ray fluorescence (XRF) core scanning is a non-destructive analysis that provides a fast analysis of major and minor element intensities. The whole suite of elements between Aluminum and Uranium was measured with an AVAATECH core scanner in two separate runs (10 kV, 0.25 mA, 20 s; 50 kV, 1 mA, 20 sec). Magnetic susceptibility (MS) was measured with a Geotek Multi-Sensor Core Logger. The core logger is equipped with a coil sensor (Bartington MS2C, 140 mm diameter) and operates at a frequency of 565 Hz and with an effective resolution of $2\ 10^{-6}$ SI units.

Vane shear strength was determined using an ASTM D4648 Wykeham-Farrance Laboratory Vane Shear Apparatus (Table 2). A four-bladed vane (12.7 x 12.7 cm) was inserted into the split core and rotated to cause a cylindrical surface to be sheared by the vane. The torque was applied through a calibrated torsion spring (type 994 number 4) and is a relatively direct measure of the sediment shear strength if normalized to the vane constant (2,68 10^{-6} m^3).

Radiocarbon dating of was carried out at the Poznań Radiocarbon Laboratory, Poland (Table 3). Raw ^{14}C ages were converted into 1-sigma calibrated ages using the Calib 7.1 software and the Marine13 calibration data set (Stuiver et al., 1998; Reimer et al., 2013) including a reservoir age of 71 ± 21 pooled from several Delta R values in the southern Barents Sea (Mangerud et al., 2006). All ages are given in calibrated kilo-years before present (cal ka BP). The median of the probability distribution is used as a reliable estimation of the sample's calendar age (Telford et al., 2004). Raw ^{14}C ages of Rüther et al. (2012) and Rebesco et al. (2016a) were re-calibrated accordingly (Table 3).

4. Sedimentary architecture of the Kveithola area

The identification of the main stratigraphic units is a prerequisite for a structured interpretation of the results. After a brief overview on the local seafloor topography, acoustic units were defined by the description of acoustic facies. Sediment cores provided insight into the sedimentary characteristics of these acoustic units. The resulting combination of acoustic and lithological data led to a determination of main units as described in the following.

4.1 Spitsbergenbanken

Within the study area, the seafloor topography of the bank surrounding the Kveithola Trough is highly differentiated (Fig. 2). The western part, including coring sites 17631 and 17630, shows a wavy seabed with less than 200 m wide reliefs of only a few meters depth (with a maximum of 6 m at site 17631). The eastern shallower part of the bank shows a generally flat topography with some larger morphological depressions, e.g., at site 17629 with a width of 1.5 km and a depth of 20 m.

Unit **B6** represents the deepest, thus oldest unit visualized by the acoustic data (Fig. 2). It is continuously present on the bank. Its total thickness remains unknown due to limited acoustic penetration. B6 is internally transparent over large parts, which does not allow for further subdivision of this unit. The upper boundary of B6 appears prolonged and highly irregular due to V- and U-shaped channel incisions. Sediment core 17630-2 reached the upper boundary of B6 but did not penetrate into this unit.

Unit **B5** occurs only in a major morphological depression that hosts site 17629 (Fig. 2). The unit shows a maximum thickness of 9 m and undulating parallel internal reflections, partly onlapping onto the boundary to Unit B6 at the depression flanks. The upper boundary of B5 appears concordant in the center of the depression, but truncated at western and eastern flanks. Core 17629-2 recovered B5 sediments (Fig. 3). Magnetic Susceptibility (MS) values are high showing an average of 235 10^{-6} SI Units. The sediment is composed of clayey silt and the portion of the fine fraction (< 63 µm) shows, with average values of 99%, the highest mud content of all stratigraphic units found on the bank. A slight coarsening-upward trend in B5 is accompanied by a slight increase in both magnetic susceptibility and carbonate content, the latter showing generally low values of 3 to 5%. In radiographic images, B5 displays fine lamination without bioturbation (Fig. 4A). Very few mm- to cm-sized lithic fragments occur throughout. Radiocarbon dating revealed an age of 16.1 cal ka BP at the top of B5 (Table 3).

Unit **B4**s is of very variable thickness, and appears in the acoustic data semi-transparent or shows a chaotic pattern of prolonged reflections. Therefore, no terminations can be determined at its upper and lower boundary (Fig. 2). Below about 145 m water depths, B4 forms a continuous cover in the western part of the investigated bank area (Fig. 2). Maximum thickness of this unit is 8 m here. Above a water depth of 143 m, B4 is only found in topographical depressions such as at site 17629 where it has a maximum thickness of 6 m in the center. Core 17629-2 stems from the depression's margin and recovered 2.8 m of B4 (Fig. 3). MS values range from 75 10^{-6} to 305 10^{-6} SI units and show an upwards decreasing trend. In core 17631-2, a sudden change towards lower MS values occurs at

3.86 m. Below 3.86 m, B4 sediments also display higher shear strength than above (Table 2; Fig. 3). In general, B4 contains mud and muddy fine sand. The fine fraction content ranges from 64 to 99%, hence displaying a much wider range in grain size than found in unit B5 (97-100%). The carbonate content shows an upwards increasing trend and ranges between 4 and 12%. Whereas the radiographic images of underlying B5 reveal a distinct fine lamination and only few rock fragments, B4 shows crude lamination throughout and a common occurrence of dispersed mm-to cm-sized lithic fragments (Fig. 4B). Radiocarbon dating on B4 sediment revealed ages of 13.5 (17630-2, 85-95 cm) and 11.8 cal ka BP (17631-2, 331-332 cm; Table 3). Sedimentation rates reach from 10 cm ka^{-1} (17630-2) to 77 cm ka^{-1} (17631-2) below 143 m water depths, and 123 cm ka^{-1} in the morphological depression at site 17629.

Unit **B3** is restricted to minor and major topographical depressions on the bank as it is the case at sites 17631 and 17629 (Fig. 2). At all these locations the unit is characterized by high-amplitude, prolonged reflections, especially at site 17631, where B3 fills a small U-shaped depression (4 m deep, 50 m wide). The upper boundary of B3 is often too close to the seafloor to be imaged separately with respect to the vertical resolution of the echosounder. A pronounced peak in MS marks the lower boundary of B3 in the sediment cores (Fig. 3). B3 shows significantly decreased grade of grain-size sorting in the fine fraction (17631-2) compared to the underlying unit B4 (Fig. 3). The carbonate content ranges between 6 and 20%. Radiographic images show a facies comparable to B4 with the exception of the presence of pyritized micro-burrows (*"Mycellia" sensu* Blanpied and Bellaiche, 1981; Fig. 4C, D). Sedimentation rates are significantly lower than in B4 and reach a maximum value of 54 cm ka^{-1} (17631-2).

Units **B2** and **B1** mostly form a less than 1-m thick drape on the bank, but since this thickness is close to the vertical resolution of the echosounder and the seafloor appears prolonged, it is impossible to differentiate B2 and B1 in the acoustic data (Fig. 2). However, the sedimentary properties of these two units clearly show substantial differences (Fig. 3). The greenish gray bioclast-rich sand of B2 abundantly contains larger components (bivalve shells of up to 6 cm in size, cm-sized mollusk shell fragments and rock fragments). These coarser components substantially decrease in number towards the overlying B1, which is also composed of bioclast-rich silty sand. Both B2 and B1 show lower MS values than all other units on the bank, and the average values in B2 (85 10^{-6} SI units) are substantially higher than those of B1 (35 10^{-6} SI units). The high content in biogenic carbonate shells and shell fragments in both units results in low average percentages of the fine fraction (B2 13%, B1 9%) and high carbonate contents (B2 46%, B1 44%) compared to the other units. Radiocarbon dating of B2 and B1 revealed ages of 8.8

(17630-2, 62-65 cm) and 3.5 cal ka BP (17631-2, 111-112 cm), respectively (Table 3). Sedimentation rates are highly valuable (B2: 4-15 cm ka^{-1}; B1: 2-77 cm ka^{-1}).

4.2 Kveithola Trough

Compared to the variable topography of Spitsbergenbanken the seafloor inside the Kveithola Trough is rather smooth. Most prominent morphological features are mega-scale glacial lineations (MSGLs), transverse grounding-zone wedges (GZWs), and two mounded depocenters that are morphologically separated from the northern wall of the Kveithola Trough by a moat (Figs. 5 and 6). These elevated depocenters were previously interpreted as current-induced shallow-water contourite drift bodies, called the Kveithola Drift (Rüther et al., 2012; Bjarnadóttir et al., 2013; Rebesco et al., 2016a). At the northeastern margin of the trough, a north-south directed structural channel is present (Fig. 1; Gabrielsen et al., 1990; Fohrmann, 1996; Fohrmann et al., 1998; Bergh and Grogan, 2003). This channel holds a minor, supposedly current-induced sediment depocenter (Hanebuth et al., 2013; Zecchin et al., 2016).

Unit **T6** forms the acoustic basement in the study area. This unit appears widely transparent with scarce internal reflections (Figs. 5 and 6). T6 is overlain by Unit **T5**, a drape with parallel reflection pattern and a relative consistent thickness of 15 m showing conformable lower and upper boundaries (Figs. 5 and 6). Reflection amplitudes and spacing change vertically. This drape also covers both flanks of the Kveithola Trough.

Units T4 to T1 form the Kveithola Drift (cp. Rebesco et al., 2016a). The internal architecture of this depocenter shows sub-parallel reflections with a remarkable thickening towards the north. These internal strata show rapidly convergent pattern at the northern-end termination and onlap onto Unit T5 beneath the moat. Whereas this east-west directed channel is well-developed at the foot of the northern flank of the trough, the southern portion of the Kveithola Drift is characterized by a persistent thinning towards the higher part of the trough's shoulder, mainly due to thinning and even termination of units T3 and T2 (Figs. 5 and 6). In the southern part of the drift Unit T3 is erosionally truncated at the top. Sediment cores from the Kveithola Drift show a common pattern in terms of sediment composition, which allows for a robust correlation between the individual cores. All cores show a pronounced MS drops from higher values in T4 and T3 towards a stable level of low intensity in T1 (Figs. 7 and 8).

Sediment cores 17612-4, 17614-2, and 17620-2 recovered the lowermost unit of the Kveithola Drift (**T4**; Figs. 5 and 6). This unit is characterized by the highest MS values values (around 110 10^{-6} SI) and a relatively low Ca/Fe ratio

(<1; Figs 7 and 8), which both hint to a relative high proportion of terrigenous/siliciclastic material. A poorly sorted and multi-modal grain-size spectrum with modes below 10 μm is found here (Figs. 7, 8, and 9) and supported by a high Al/Zr ratio as an indicator for fine sediment. Radiocarbon dating provided ages of 13.0 (17614-2, 287 cm), 12.6 (17612-4, 269-270 cm), 12.1 (17620-2, 480 cm), and 11.2 cal ka BP (17612-4, 185-186 cm; Table 3). Sedimentation rates increase from south to north from 53 cm ka^{-1} (17614-2) and 60 cm ka^{-1} (17612-4) to 134 cm ka^{-1} (17620-2).

The overlying Unit **T3** shows MS signals steadily decreasing upcore from about 100 to 40 10^{-6} SI units (Figs. 7 and 8). This decrease is accompanied by low, slightly rising Ca/Fe ratios (from <1 to 2), suggesting a strong influence of siliciclastic components. The grain-size distribution changes gradually towards a coarser mode of the spectrum (from about 50 to 105 μm; Figs. 7, 8, and 9). The fine modes, observed in unit T4, fade out gradually. This overall coarsening trend is corroborated by decreasing Al/Zr values. A radiocarbon age of 10 cal ka BP was measured in this unit (17607-5, 919-920 cm; Table 3). Sedimentation rates show a comparable pattern as in T4 with increasing rates towards the north from 35 cm ka^{-1} (17612-4) to 138 cm ka^{-1} (17620-2).

A sharp contact defines the base of the following drastically different unit. The entire system experiences an establishment of a dominant coarse grain-size mode in Unit **T2** (Figs. 7 and 8). This mode finalizes the overall coarsening upward trend observed in the preceding T3. T2 is characterized by a stepwise change in the parameters: MS shows a rapid decrease in intensity towards a low level (40-45 10^{-6} SI), Ca/Fe indicates carbonate-related positive peaks, and Al/Zr resembles the positive correlation between a comparably good grain-size sorting and a coarser sediment composition (Figs. 7, 8, and 9). Radiocarbon ages reach from 8.8 cal ka BP (17619-3, 497-498 cm) to 6.3 cal ka BP at the boundary to the overlying Unit T1 (17607-5, 575-577 cm; Table 3). Whilst the sedimentation rate of T2 generally increases from south to north (from 33 cm ka^{-1} in core 17612-4 to 78 cm ka^{-1} in core 17607-5), the core taken from the northernmost part of the depocenter (17620-2) shows a drastically reduced sedimentation rate of 6 cm ka^{-1}.

The youngest Unit **T1** shows a relative homogenous appearance. MS shows consistent and weak signals below 40 10^{-6} SI units, with a higher excursion in the uppermost layer (Figs. 7 and 8). The Ca/Fe ratio indicates an important though variable contribution of marine biogenic carbonate, decreasing towards the top. The grain-size distribution displays a robust coarse-grained signal throughout (Figs. 7 and 8). The two fine-grained modes at 6-8 and 20-25 μm are much more pronounced than in T2 but the well-defined coarse peak (50-105 μm) remains dominant (Fig. 9). The comparably low Al/Zr ratio supports this observation. T1 formed during the past 6.3 cal ka BP (Table 3). The distribution of sedimentation rates is comparable to T2 with generally increasing rates from south to north (2 cm ka^{-1} in core 17612-4; 91 cm ka^{-1} in core 17607-5) and drastically reduced sedimentation rate of 2 cm ka^{-1} close to the moat (17620-2).

The grain-size measurements do not only reveal temporal changes in grain size but do also allow to investigate lateral trends across the Kveithola Trough. Cores 17612-4, 17613-2, and 17607-5 describe a transect from the southern shoulder of the Kveithola Trough towards the main center of the sediment drift (Fig. 7). The core closest to the shoulder (17612-4) does not only show the lowest overall sedimentation rates (21 cm ka^{-1}), more than 4 times lower than that found in the central core 17607-5 (92 cm ka^{-1}), but also contains the coarsest material. Pronounced grain-size modes in core 17612-4 occur at around 105, 20 and 7 μm, in core 17613-2 at 70, 20 and 7 μm, and in core 17607-5 at 50, 20 and 7 μm (Figs. 7 and 9). Hence, the laterally fining trend towards the north is exclusively related to the coarsest mode. The same is the case for the second transect across the sediment drift located further east. The two finer modes in cores 17614-2, 17619-3, and 17620-2 show relatively consistent values at 6-8 and 20-25 µm (Fig. 8). The coarsest mode, however, displays a significant northward fining from 95 µm in core 17614-2 to 65 µm in core 17619-3 to 50 µm in core 17620-2, which is corroborated by a general decrease of reflection amplitudes to the north in the sediment echosounder data. The fact that the coarse mode shows a consistent change across the two transects but the two finer modes are conservative throughout the system suggests different transport mechanisms and/or material sources for the coarser and the finer components as discussed in Section 6.2.

5. Interpretation

5.1 Determination of paleo-environments

5.1.1 Spitsbergenbanken

B6 extends below the maximum coring penetration depth (Fig. 2). The age of the overlying units (see below), the irregular upper boundary, the largely transparent character of the acoustic facies, and the fact that the vibrocorer got stuck on its surface, altogether suggest that this unit consists of subglacial till of Late Weichselian age, as described by other authors (Bjørlykke et al., 1978; Elverhøi et al., 1998; Elverhøi and Henrich, 2002). The few internal reflections might point to different phases of ice advance and retreat.

The occurrence of laminated mud (**B5**) is unprecedented on the bank areas that surround the Kveithola Trough. The preservation of well-developed rhythmic patterns points to high sedimentation rates and absent bioturbation (Fig. 4A). A low carbonate content is most probably the result of massive supply of terrigenous sediments (Fig. 3). Comparable laminated sediments were reported from the glaciomarine blanket inside the Kveithola Trough (Rüther et al., 2012; Bjarnadóttir et al., 2013) and from the Kveithola Trough Mouth Fan (Blaume, 1992; Lucchi et al., 2012, 2013). The deposits were interpreted as the product of rapid settling from suspension clouds that originated during an early phase of deglacial retreat of the Svalbard-Barents Sea Ice Sheet (SBIS; Elverhøi et al., 1995; Svendsen et al., 1996; Jessen et al., 2010) and were referred to as "plumites" (Hesse et al., 1997; Rüther et al., 2012; Lucchi et al., 2013, 2015). Hence, B5 represents a glaciomarine facies of regional extent in proximal position to the SBIS. Low IRD contents were previously related to the presence of a semi-permanent sea-ice cover that widely prevented extensive iceberg rafting (Vorren et al., 1984; Forwick and Vorren, 2009; Dowdeswell et al., 1998).

Sediment lamination and a high terrigenous content characterize both B5 and B4 (Figs. 3 and 4A, B). The lamination in **B4** is, however, mostly crude, the grain size is coarser, IRD is abundant throughout, and the biogenous carbonate content is higher than in B5. The presence of crude lamination indicates a persisting impact of sediment-rich meltwater plumes derived from the SBIS, on the one hand. On the other hand, occasional ploughmarks, chaotic acoustic patterns, and a rich IRD content are a result of intense iceberg keel scouring. B4 is therefore interpreted to have formed in a relatively larger distance from the SBIS than it was the case for B5, i.e. the ice sheet retreated remarkably but was still close enough to supply significant amounts of material through meltwater plumes.

The small-scale U-shaped depression at site 17631 indicates one of these iceberg ploughmarks (Fig. 2). The sediment fill (**B3)** shows parallel internal acoustic patterns. Since ploughmarks are absent in the large depression on the southeastern part of the bank in the study area (site 17629), deposition of B3 in this particular area was unaffected by iceberg keel scouring. The sedimentary properties of B3 and B4 are, with the exception of pyritized micro-burrows, comparable (Fig. 4C, D). Therefore, both units were influenced by sediment supply from the melting ice sheet.

The marked decrease in MS at the boundary between B3 and B2 is linked to higher amounts of coarse-grained carbonate shells and a lower content of fine-grained terrigenous sediment (Fig. 3). Due to the dominance of bioclast-rich sand and gravel (shells and rock fragments) **B2** shows a typical characteristic of a lag deposit caused by intense winnowing related to strong bottom currents. Comparable lag deposits were reported from Spitsbergenbanken by Bjørlykke et al. (1978), Henrich et al. (1997), and Elverhøi and Henrich (2002).

B1 is composed of a modern bioclastic-rich sand. The finer grain size compared to B2 points to a decrease in bottom current intensity. A comparable carbonate sand cover overlying a lag deposit was also observed in other shallow parts of the NW Barents Sea (Bjørlykke et al., 1978; Henrich et al., 1997; Elverhøi and Henrich, 2002).

5.1.2 Kveithola Trough

T6 is interpreted to include transversal wedges extending over the whole width of the trough (Fig. 1). These grounding-zone wedges formed by deposition of subglacial till material during temporary stillstands of the ice-stream front (Dowdeswell et al., 2008; Ò Cofaigh and Stokes, 2008; Rebesco et al., 2016b). Therefore, T6 consists of subglacial tills and formed during different phases of ice advance and retreat. Rüther et al. (2012) and Rebesco et al. (2016a) suggest a late-Weichselian age for such subglacial deposits.

T5 overlies the subglacial deposits of T6. T5 shows a relative constant thickness across the trough and represents a sediment drape (Figs. 5 and 6). These minor thickness variations and parallel reflection patterns suggest uniform and widespread sediment supply. Rebesco et al. (2011, 2016a), Rüther et al. (2012), and Bjarnadóttir et al. (2013) described the sediments of the glacigenic blanket in the Kveithola Trough as plumite deposits and layered diamicts, which represent intense iceberg rafting due to the initial disintegration of the SBIS.

Units T4 to T1 were recovered by the sediment cores of this study (Figs. 7 and 8). These units form a contourite drift in the Kveithola Trough (Figs. 5 and 6; Rüther et al., 2012; Bjarnadóttir et al., 2013; Rebesco et al., 2016a). The stratigraphically deepest of these four units (**T4**) shows a dominance of fine modes (20-25 µm and 6-8 µm; Fig. 9) and highest terrigenous material proportions in the succession (Figs. 7 and 8). The grain-size distribution displays a uniform lateral signal without a notable gradient. This observation in addition to a relatively poor degree in sediment sorting suggests calm hydrodynamic conditions favoring vertical particle settling. In contrast to the underlying glacigenic blanket (T5), T4 pinches out towards the trough's southern margin (Figs. 5 and 6), which suggests that a yet undescribed localized bottom current started to affect this zone resulting in non-deposition and erosion (see section 6.1). According to the sediment-acoustic geometry as well as from the slightly better sorted grain-size spectrum at site 17620, the moat at the northern margin of the trough started to serve as an active pathway for brine-enriched shelf waters (Rebesco et al., 2016a). These dense waters were reported to follow the wavy lateral geometry of the moat, a feature that was discussed in detail by Rebesco et al. (2016a).

The following phase shows a continuous intensification of the transport energy illustrated by general coarsening trends at all sites (**T3**; Figs. 7, 8, and 9). A major spatial differentiation in material developed during this time. A conspicuous lateral gradient led to significant material coarsening in proximity to the trough's southern flank and with finest sediments depositing close to the moat. This distribution indicates that the moat, though playing an important role in shaping the drift-like depositional geometry, was not the source for the material involved in the coarsening trend towards the south. Thus, a second sediment source needs to be considered supplying material over the southern flank of the Kveithola Trough, which led to a significant lateral sorting effect with coarser material depositing more proximal, i.e. close to the flank. This source was most probably the southern bank (see Section 6.2). The fact that all data characterizing T3 show a clear shift towards higher bottom current energy and increased biogenous carbonate content points to a strongly reduced influence of the SBIS on the deposition in the study area.

A major change in the trough's sedimentation regime, thus in the bottom current system, started with the onset of **T2**. Acoustic data shows an erosional contact between T3 and T2 (Figs. 5 and 6) and a coarse and comparably sorted grain-size signal dominated the deposition over the whole trough (Figs. 7, 8, and 9). The lateral northward fining observed in underlying T3 is also true for T2, which implies continued sediment supply from the southern bank. The trough-wide coarsening at the border between T3 and T2 would therefore imply that the bottom currents on southern Spitsbergenbanken intensified significantly during this time.

Unit **T1** shows a general trend towards lower Ca/Fe values in the upper part of this unit, reflecting either stronger terrigenous supply or reduced marine primary productivity (Figs. 7 and 8). A decreasing dominance of the coarsest grain-size mode (Figs. 7, 8, and 9) is probably related to a decrease in supply of coarser material from the Bank. This decreasing supply points to a general weakening of the bottom currents on the bank and at the southern flank of the trough, compared to the T2 time interval. The minor sedimentary changes within T1 indicate that the modern hydrodynamic and sedimentary systems established at around 6.3 cal ka BP.

5.2 Stratigraphic relationship between bank and trough environments

Previous studies of Rüther et al. (2012) and Rebesco et al. (2016a) provided a comprehensive stratigraphic framework for the Kveithola Trough based on seismo-acoustic data, lithological characterization, and radiocarbon dating. The compilation of radiocarbon dates from Rüther et al. (2012), Rebesco et al. (2016a), and our study reveals six time intervals: >16.1, 16.1-13.5, 13.5-11.2, 11.2-8.8, 8.8-6.3, and 6.3-0 cal ka BP (Fig. 10). Both bank and trough units were correlated based on magnetic susceptibility and grain-size distribution curves within the age framework from radiocarbon dating (Fig. 11).

> 16.1 cal ka BP

Inside the Kveithola Trough, subglacial deposits of Late Weichselian age were observed by, e.g., Vorren and Laberg (1996), Rebesco et al. (2011, 2016a), Rüther et al. (2012), and Bjarnadóttir et al. (2013). On Spitsbergenbanken, the presence of Late Weichselian subglacial deposits was also described by various authors (Bjørlykke et al., 1978; Henrich et al., 1997; Elverhøi and Henrich, 2002). For instance, Bjørlykke et al. (1978) identified Mesozoic lithic fragments in Holocene lag deposits and suggested that these fragments stem from underlying moraines. However, the age of the boundary between subglacial deposits and the initial formation of the glaciomarine blanket, i.e. the timing of ice retreat, remained unclear (Fig. 10). Our acoustic dataset reveals subglacial deposits on the bank (**B6**) and in the trough (**T6**) that form the foundation for the subsequent deglacial units (Fig. 11). The new radiocarbon age of 16.1 cal ka BP from B5 (see next section) indicates that subglacial deposition occurred significantly earlier than the previously suggested 14.6 cal ka BP (Rüther et al., 2012).

16.1-13.5 cal ka BP

Plumites occur on the bank (**B5**) and inside the trough (**T5**; Fig. 11). Plumites in the Kveithola Trough are part of the glacigenic blanket previously interpreted by Rebesco et al. (2011, 2016a; Units 1a and 1b) and Rüther et al. (2012; Unit CU3; Fig. 11). Published radiocarbon ages range between 14.4 and 13.9 cal ka BP (Rüther et al., 2012; Fig. 10) and the formation of this blanket took place over large parts of the Bølling-Allerød interstadial (14.7 to 12.7 cal ka BP; Cronin, 1999). Since plumites from the bank and trough deposited in close proximity to each other, only a slight delay in the timing of the meltwater contribution should be expected between bank and trough, if at all. Plumite deposition in the major depression on the bank and the glacigenic cover in the trough would therefore be synchronous (Fig. 11). The radiocarbon age of 16.1 cal ka BP indicates that plumite deposition in the study area occurred 1.5 thousand years earlier than previously assumed (Figs. 10 and 11). Hence, the boundary between subglacial deposits and glacigenic blanket has a minimum age of 16.1 cal ka BP.

13.5-11.2 cal ka BP

The initial formation of a sediment drift in the Kveithola Trough occurred between 13.9 and 13.1 cal ka BP (CU2, Rüther et al., 2012; Unit 2a and 2b, Rebesco et al., 2016a; Fig. 10). Our radiocarbon age of 13.5 cal ka BP on Spitsbergenbanken corroborates the timing of the onset of B4 and T4 between 13.9 and 13.1 cal ka BP. Additional radiocarbon ages on both bank and trough deposits clearly indicate that **B4** and **T4** formed synchronously to Units CU2, 2a and 2b (Fig. 10). Therefore, large parts of B4 and T4 formed during the Late Bølling-Allerød interstadial (14.7 to 12.7 cal ka BP; Cronin, 1999) and the Younger Dryas stadial (12.8-11.7 cal ka BP, Broecker et al., 2010).

11.2-8.8 cal ka BP

Rüther et al. (2012) proposed a change from CU2 to CU1 at 11.2 cal ka BP based on a lithofacies change from layered diamict and massive to crudely stratified mud to crudely laminated, bioturbated mud. While the boundary between CU2 to CU1 could not be determined from the chirp data, acoustic investigations and a radiocarbon date from Rebesco et al. (2016a) confirmed the exact age of the transition from CU2 to CU1 at 11.2 cal ka BP (time equivalent to the boundary between Units 2b and 3a ; Figs. 10 and 11). Other radiocarbon measurements on these units revealed ages of around 10 cal ka BP (Fig. 10). Hence, the formation of CU1 and Unit 3a occurred during the Preboreal-Boreal time interval (11.6-9.2 cal ka BP; Cronin, 1999). The linkage of **B3** with **T3** is based on correlations of the MS curves and indicates a time-equivalent formation to CU1 and Unit 3a (Figs. 10 and 11).

8.8-6.3 cal ka BP

A "Sandy Unit" (bioclast rich sand and silt) caps CU1 at 8.8 cal ka BP (Rüther et al., 2012), time equivalent to the transition from Unit 3a to 3b between 10 and 8.8 cal ka BP (Rebesco et al., 2016a; Fig. 10). Likewise, a significant and abrupt coarsening of both bank and trough deposits marks the onset of **B2** and **T2** (Fig. 11). A radiocarbon age on Spitsbergenbanken corroborates the onset of the coarsening at around 8.8 cal ka BP (Fig. 10). Although the observed lag deposit on the bank is in agreement with findings by other studies, radiocarbon dates vary largely. According to Hald and Vorren (1984) the onset of bioclastic-rich sedimentation on the bank occurred at 7.8 cal ka BP. Henrich et al. (1997) related the formation of the lag deposit to 8-3 cal ka BP and Elverhøi and Henrich (2002) proposed an interval from 8 to 4 cal ka BP for its formation. Although radiocarbon dating was often performed on surface samples, maximum ages of around 8 cal ka BP roughly fit the onset of lag deposition at around 8.8 cal ka BP. The sharp basal boundaries of B2 and T2 imply high-energy conditions, which agrees to observations of an erosional surface at the base of Unit 3b defined by Rebesco et al. (2016a). The start of their Unit 3b was tentatively assigned to the onset of a short-lasting atmospheric cooling event at 8.8 cal ka BP, as reported by Sarnthein et al. (2003) and Hald et al. (2007). The age of the upper boundary of Unit 3b remains undated (Fig. 10).

6.3-0 cal ka BP

The shift from T2 to T1 and B2 to B1 occurred at 6.3 cal ka BP, i.e. in the middle Holocene (8.2-4.2 cal ka BP; Walker et al., 2012; Fig. 10). According to our correlations, B1 and T1 comprise the upper part of Unit 3b and the entire Unit 4 of Rebesco et al. (2016a; Figs. 10 and 11). These authors define the boundary between Units 3b and 4 by a slight change in magnetic susceptibility. However, this boundary lacks any other significant sedimentary changes. Conversely, an abrupt shift in grain size at 6.3 cal ka BP represents the base of T1 and B1.

6. Discussion

Although contrasting depositional processes control the environments on the bank and in the trough, the reliable temporal and spatial correlation of bank and trough units suggests that the significant environmental changes along the defined time intervals are a result of regional external forcing mechanisms, as discussed in the following.

6.1 Deglacial retreat dynamics of the Svalbard-Barents Sea Ice Sheet

> 16.1 cal ka BP

Subglacial deposits in the study area indicate a dominant control of glacial ice sheet dynamics on the sediment distribution. . A grounded ice sheet covered Kveithola Trough and surrounding Spitsbergenbanken suppressing shelf water circulation. The oldest signs of a glaciation of the western Svalbard margin were reported to have occurred at around 2.3 Ma (Faleide et al., 1996; Forsberg et al., 1999) and the last major ice extension of the Svalbard-Barents Sea Ice Sheet (SBIS) appeared during the Late Weichselian glaciation (Vorren and Laberg, 1996; Landvik et al., 1998; Patton et al., 2015, 2016; Newton and Huuse, 2017). Full glaciation of the western Svalbard shelf was achieved by about 24 cal ka BP (Jessen et al., 2010) and large volumes of meltwater, sediments, and IRD were delivered to the shelf break by major ice streams (Batchelor and Dowdeswell, 2014; Ottesen et al., 2002; Andreassen et al., 2008; Patton et al., 2015, 2016). Radiocarbon dates from the Bear Island Trough area indicate that the Late Weichselian ice stream reached the shelf edge twice, first prior to 22 cal ka BP and second after 19 cal ka BP (Sættem et al., 1992; Laberg and Vorren, 1995). Brendryen et al. (2015) reported several ice advances onto the northern Norwegian shelf during the Late Weichselian and relate these advances to cold periods with low influx of Atlantic Water.

16.1-13.5 cal ka BP

The occurrence of plumites on the bank indicates the retreat of the SBIS and the related release of suspension-rich meltwater plumes in the study area. Inside the trough, comparable laminated fine sediments form the youngest part of the widespread glacigenic blanket (Rüther et al., 2012; Bjarnadóttir et al., 2013). The bank lacks such a widespread distribution of plumites and these laminated deposits are restricted to deeper bank areas, i.e. the topographical depression in the southeastern study area. Hence, bottom currents affected shallower areas of the bank, which led to bypassing of these fines. Deeper areas offered protection from stronger currents thereby representing exceptional areas for plumite deposition and their later preservation.

Plumite deposits of the study area contain low amounts of IRD. Relatively low IRD concentrations in Storfjorden Shelf sediments during the same time interval were related to suppressed ice rafting due to an almost permanent sea-ice cover (Rasmussen et al., 2007; Fig. 12). Much higher IRD concentrations in the W Spitsbergen region from 17.5 to 14.5 cal ka BP (Ślubowska-Woldengen et al., 2007; Fig. 12) indicate that intense iceberg rafting and related massive supply of IRD appeared earlier than it was the case for Kveithola and Storfjorden areas. This massive supply of IRD might have originated from a fast flowing ice stream out of Isfjorden Trough (Andersen et al., 1996).

Deglaciation of the western Svalbard shelf break appeared at 20.5 cal ka BP based on the onset of hemipelagic sedimentation in Storfjorden Trough at 19.6 cal ka BP and high IRD concentrations between 21.2 and 19.8 cal ka BP (Rasmussen et al., 2007; Jessen et al., 2010; Patton et al., 2015, 2016). Svendsen and Mangerud (1992) and Ebbesen et al. (2007) reported an overall decrease in meltwater and a rapid retreat of the glaciers on western Svalbard for the Bølling-Allerød time interval (14.7 to 12.7 cal ka BP; Cronin, 1999), coinciding with the abrupt warming recorded in Greenland (Johnson et al., 2001). Elverhøi et al. (1993) suggested that significant parts of the Barents Sea were deglaciated at 15 cal ka BP. The initial ice-stream retreat in the Kveithola region was suggested by Bjarnadóttir et al. (2013) to be contemporaneous to the onset of deglaciation in the Storfjorden Trough that took place at about 20-19 cal ka BP (Rasmussen et al., 2007; Jessen et al., 2010; Lucchi et al., 2013, 2015; Rigual-Hernández et al., 2017). Rüther et al. (2012) suggested that plumites in the Kveithola Trough deposited before 14.2 cal ka BP. The actual timing of early deglaciation of the study area remains rather unclear. Our new radiocarbon age retrieved from the top of plumite deposits on Spitsbergenbanken indicates that such laminated sediments formed already at 16.1 ka BP (Fig. 3). Hence, the major disintegration of the SBIS in the study area occurred earlier than 16.1 cal ka BP, at least 1.4 ka before the start of the Bølling-Allerød time interval. Hence, melting dynamics of the proximal ice sheet controlled the sedimentation in the study area and meltwater plumes were the dominant sediment source. Following the early break apart, the SBIS experienced an ongoing disintegration during late Bølling/Allerød until only minor parts of Spitsbergenbanken were still covered by a grounded ice sheet (Siegert and Dowdeswell 2002; Ślubowska-Woldengen et al., 2008; Winsborrow et al., 2010).

13.5-11.2 cal ka BP

From 13.5-11.2 cal ka BP, higher amounts of IRD compared to underlying plumite deposits indicate enhanced iceberg rafting and diamict deposits. The occurrence of mud interlayered into these debris successions indicates an ongoing terrigenous supply by meltwater plumes. Hence, although the ice sheet on Spitsbergenbanken disintegrated into the Scandinavian and Svalbard ice sheets between 15-12 cal ka BP (Siegert and Dowdeswell, 2002; Newton and Huuse, 2017) and grounded ice was limited to the area south of Svalbard (Mangerud and Landvik, 2007; Rüther et al., 2012), sediment supply in the study area was still tightly connected to the ice-sheet melting dynamics. The observation of increased ice rafting in the study area coincides to increased IRD contents on the Storfjorden shelf from 13.5-11 cal ka BP (Rasmussen et al., 2007; Fig. 12).

Although both bank and trough show comparable sedimentary facies during the two time intervals from 13.5 to 11.2 cal ka BP and 11.2 to 8.8 cal ka BP (mostly showing crudely laminated mud and diamicts with muddy matrix), the depocenter shapes are completely different. Bank deposits show irregular lateral thickness and occasional U- and V-shaped incisions caused by syn- and post-depositional iceberg-keel scouring (Zecchin et al., 2016). A further indication on the bank for the presence of SBIS disintegration are higher shear strength values at the base of B4, most probably due to compaction by iceberg-seabed interaction. At the same time, the contourite drift started to form inside the Kveithola Trough. This drift was reported to show an onset at about 13 cal ka BP (Rüther et al., 2012; Rebesco et al., 2016a). The bottom current shaping this confined depocenter was presumably related to the formation of brine-enriched shelf waters cascading from Spitsbergenbanken downward into the trough (Fohrmann, 1996; Fohrmann et al., 1998; Rebesco et al., 2016a). **6.2 Holocene evolution of bottom current strength**

11.2-8.8 cal ka BP

On the bank, the Early Holocene time interval was still characterized by the deposition of interlayered mud and diamicts that are present at site 17629 and as ploughmark fill at site 17631. Nevertheless, the strong decrease in IRD contents on the Storfjorden shelf indicates a significantly reduced impact of the ice sheet on the sediment distribution in the western Barents Sea area (Rasmussen et al., 2007; Fig. 12). Despite these features, a systematic coarsening trend characterizes deposits on the bank and inside the trough (Fig. 12). This grain-size change indicates a transition towards stronger bottom currents and, therefore, increased winnowing and off-bank transport of coarse sediments. Such a system-wide coarsening trend indicates a major change in the regional oceanographic configuration. The ongoing decay of the grounded ice sheet on the Barents Shelf led to a first opening of an ocean passage between eastern Svalbard and Nowaja Semlja in the early Holocene (Siegert and Dowdeswell, 2002), thus allowing for an exchange between the Norwegian Sea and the Arctic Ocean across the Barents Shelf. Sea-surface temperatures off western Svalbard and in the Barents Sea rose abruptly (Birks and Koç, 2002; Sarnthein et al., 2003; Hald et al., 2007; Forwick and Vorren, 2009), defining the regional Thermal Maximum. This warm phase was accompanied by a strong North Atlantic Current and a stable Polar Front preventing the intrusion of cold waters from the north (Hald et al., 2007). The gradual northward displacement of the Polar Front, separating Arctic and Atlantic water masses, led to an enhanced influence of warm Atlantic Water in the study area (Hald et al., 2007; Carbonara et al., 2016; Bøe et al., 2017; Rigual-Hernández et al., 2017). A related increase in bottom current strength of the Atlantic Water flow should have resulted in an intensification of off-bank export of coarser sediments and could represent the main reason for the gradual coarsening of the trough deposits.

8.8-6.3 cal ka BP

The interval 8.8-6.3 cal ka BP is characterized by the coarsest sediments in the study area (Fig. 12). The coarsening affects both terrigenous and biogenous particles. The increase of biogenous carbonate contents could be related to: (1) the successive retreat of the ice sheet that led to a significantly decreased supply of terrigenous material; and (2) the increased inflow of Atlantic Water and the establishment of an ice-free season both favoring marine biogenous production. The time-equivalent coarsening of the terrigenous fraction indicates that decreasing terrigenous supply and increasing biogenic production were not the solely reasons for the strong and abrupt coarsening at around 8.8 cal ka BP. Hence, increasing bottom current strength probably played a major role for the formation of a lag deposit on Spitsbergenbanken. Lag deposit formation on Spitsbergenbanken due to strong winnowing is corroborated by the studies of Vorren et al. (1984) and Elverhøi and Henrich (2002). Elverhøi and Henrich (2002) reported stronger bottom currents on Spitsbergenbanken from 8-4 cal ka BP. These authors relate increased current strength to a glacio-isostatic rebound of 60–100 m during the past 10 cal ka BP. The gradual shallowing caused by this glacio-isostatic rebound led to enhanced off-bank export of coarse sediments. Vorren et al. (1984) related coarser sediments on the banks off northern Norway to increased winnowing due to a Holocene intrusion of Atlantic Water. According to Ślubowska-Woldengen et al. (2008) the strongest inflow of Atlantic Water occurred in the time interval from 9.5-7.5 cal ka BP, a timing that coincides with observations of Andersen et al. (2004). These authors reported warm and stable conditions during the interval from 9.5-6.5 cal ka BP with a strong Atlantic Water current widely intruding towards the north. The time-equivalent coarsening of deposits in the Kveithola Trough would then point to winnowing of the bank and subsequent off-bank transport of the coarse sediments into the trough. This off-bank export is in agreement to observations of lower sedimentation rates in shallower areas and increased accumulation of sediments in deeper regions of the Barents Sea (Elverhøi et al., 1989; Zaborska et al., 2008). Hence, the strengthening of Atlantic Water inflow and the gradual shallowing caused by glacio-isostatic rebound might be the main reasons for the observed regional coarsening but further studies (e.g., on foraminiferal assemblages) are needed to proof this relationship.

6.3-0 cal ka BP

The grain-size change from lag deposit to bioclastic-rich sands on the bank and the decrease of sorting in the trough point towards a weakening of the hydrodynamic regime at around 6.3 cal ka BP. Vorren et al. (1978, 1984) relate such a transition during the “later part of the Holocene” to a weakening of high-energy winnowing on the banks due to the Holocene eustatic sea-level rise. In addition, warm conditions during the early Holocene were followed by an overall cooling trend (Andersen et al., 2004; Hald et al., 2007; Ślubowska-Woldengen et al., 2007). Proposed onsets of this cooling interval reach from 9 cal ka BP (western Barents Sea slope; Hald et al., 2007) to 6.8 cal ka BP (off northern Svalbard; Ślubowska-Woldengen et al., 2007) and 6.5 cal ka BP (Vøring Plateau; Andersen et al., 2004). The overall cooling was accompanied by a reduced inflow of Atlantic Water after 7.5 cal ka BP though still being stronger than during the Bølling-Allerød interval (Ślubowska-Woldengen et al., 2008). Hence, the decrease in grain size in both bank and trough records at around 6.3 cal ka BP might be related to this reduction in Atlantic Water inflow.

6.3 Implications for the shallow-water contourite concept: sediment sources and local sediment distribution mechanisms

In acoustic data, the Kveithola Drift exhibits a clearly defined moat and strata progressively thinning towards the southern flank of the trough, the latter being related to southward decreasing sedimentation rates. Therefore, this depocenter resembles the shape of a separated drift (Faugères et al., 1999; Rebesco and Stow, 2001; Stow et al., 2002; Rebesco and Camerlenghi, 2008: Rebesco et al., 2014b; Fig. 13A). This type of a contourite drift is elongated parallel to the bottom current flow direction and separated from the adjacent margin by an erosional/non-depositional moat along which the principal flow is focused (Faugères and Stow, 2008).

Three main grain-size modes characterize the composition of the drift sediments (Fig. 9). The two finer modes display a signal without significant spatial and temporal changes and, thus, seem to be independent of climatic and oceanographic changes. In contrast, the coarse mode shows a lateral coarsening trend from the moat towards the southern flank of the trough. This coarsening contradicts the concept of a separated drift, i.e. expectedly coarser-grained sediments in proximity to the moat (highest current energy) and a progressive fining with increasing distance from the moat.

According to Fohrmann (1996) and Fohrmann et al. (1998), brine-enriched shelf waters cascade from a system of channels on Spitsbergenbanken adjacent to the northern flank of the Kveithola Trough. These dense waters generate bottom currents that shaped the Kveithola Drift moat over the past 13 cal ka BP (Rebesco et al., 2016a). At least one of the three observed grain-size modes (50-105, 20-25, and 6-8 µm; Fig. 9) should be the result of these brine-enriched shelf water flows. The coarsest mode of the terrigenous grain-size spectrum (50-105 µm) shows a coarsening with increasing distance from the moat (Figs. 7 and 8). This coarsening in transport direction would contradict the concept of progressive sorting (*sensu* Swift and Thorne, 1991). Hence, one of the other two finer grain-size modes (20-25 or 6-8 µm) should be related to the bottom currents shaping the moat. The grain-size fraction 20-25 µm lies within the range of sortable silt (*sensu* McCave et al., 1995) and we suggest that this mode is related to brine-enriched shelf waters whilst the peak at 6-8 µm might stem from the hemipelagic settling of fines.

If brine-related bottom currents are not the main mechanism providing the coarse mode in grain size, another mechanism must be driving this mode and its lateral grain-size variation. Following the concept of progressive sorting (*sensu* Swift and Thorne, 1991), winnowing of deposits on the bank south of the Kveithola Trough and subsequent off-bank transport would result in coarser sediments close to the bank's margin and progressive material fining with increasing distance from the bank. Hence, the observation of lateral material fining across the drift towards the north indicates that the southern bank acted as the main sediment source for the coarse grain-size mode. Furthermore, the correlation between bank and sediment drift deposits shows coinciding trends in grain-size change, i.e. a progressive coarsening until about 8.8 cal ka BP, coarsest sediments from 8.8 to 6.3 cal ka BP, and a slight fining after 6.3 cal ka BP. These synchronous grain-size changes indicate a regional connection. Coarser intervals might be related to a strengthening of the West Spitsbergen Current carrying Atlantic Water (see Section 6.2.). According to recent studies, the branches of the West Spitsbergen Current entering the Barents Sea are capable of transporting sand (King et al., 2014; Bøe et al., 2015). In this case, Atlantic Water flow across the bank would have led to winnowing and off-bank export of coarse sediments.

Sole off-bank transport would lead to the built-up of an off-bank wedge, i.e. a northward decrease of both sedimentation rates and grain size with increasing distance from the bank margin (Fig. 13B). However, the Kveithola Drift does not show a wedge-like shape. Instead, sedimentation rates increase towards the deeper, northern part of the trough. In addition, the width of the trough limits the possible extension of the drift, which would result in a confined drift (Faugères et al., 1999; Rebesco and Stow, 2001; Stow et al., 2002; Rebesco and Camerlenghi, 2008; Rebesco et al., 2014b; Fig. 13C). The Kveithola Drift however shows neither a second moat nor higher sedimentation rates in the southern area. Hence, a more complex hydrographic forcing is needed to explain the shape of the drift (Fig. 13D, E). First, brine-enriched shelf waters formed the moat. Second, Atlantic Water flowing across the bank most probably supplied coarse sediments into the trough. Third, another branch of the West Spitsbergen Current carried Atlantic Water into the Kveithola Trough from the west (Figs. 1 and 13E; Swift, 1986; Stiansen and Filin, 2007). This branch was guided along the trough's southern flank due to Coriolis forcing, thus intensifying here. This branch did not lead to an obvious moat here but suppressed deposition (Figs. 6 and 13E). As a fourth factor, the pre-existing trough morphology clearly left an imprint in the overall geometry of the Kveithola Drift. For example, the height of the mounded center of the drift is largely enhanced by an elevation in the underlying topography (Figs. 5 and 6).

Taken all characteristics into account, we propose that the Kveithola Drift represents a combination of an off-bank wedge and a confined drift (Fig. 13D). Our findings show that a sole consideration of seismo-acoustic data might result in misleading interpretations of the forcing mechanism that shape a sediment drift. Hence, seismo-acoustic data should be accompanied by grain-size measurements on sediment cores in case the physiographic and oceanographic conditions imply a complex local to regional hydrodynamic regime. The situation described in this study may be specific for shallow-water contourite systems. In deeper waters, the situation might nevertheless be also more complicated than expected with an interaction of slope-parallel bottom currents and redirected currents inside canyons or around obstacles (e.g., Preu et al., 2013; Voigt et al., 2013; Hanebuth et al., 2015).

Conclusions

The succession of deposits on Spitsbergenbanken and in the Kveithola Trough displays exemplarily the ice retreat dynamics of the Western Barents Sea. Basal subglacial deposits formed during the Late Weichselian glaciation and the grounded ice sheet dominantly controlled their distribution. Overlying plumites are the product of rapid settling from suspension clouds that originated during an early phase of deglacial retreat of the Svalbard-Barents Sea Ice Sheet. A new radiocarbon age, retrieved from these plumite deposits on Spitsbergenbanken, indicates that the major disintegration of the ice sheet in the study area occurred earlier than 16.1 cal ka BP. Crudely laminated deposits containing abundant ice-rafted debris on the bank and inside the trough formed from 16.1 to 13.5 cal ka BP. Their origin relates to a combination of meltwater plumes, derived from the ice sheet, and intense iceberg keel rafting, both indicating a further retreat of the ice sheet.

Contemporaneous grain-size changes at all cored sites indicate that the progressive ice retreat led to an increasing impact of region-wide bottom currents on the formation of deposits on the bank and inside the trough. The time interval from 8.8 to 6.3 cal ka BP reveals the coarsest sediments in the study area including the formation of a lag deposit on Spitsbergenbanken. We relate this coarsening to a significant strengthening of bottom currents, which might be ralted to a strong inflow of Atlantic Water across the bank and into the trough.

A contourite drift formed inside the Kveithola Trough over the past 13 cal ka BP. The flow of brine-enriched shelf waters led to the formation of a moat at the northern part of the drift. Although the sediment drift resembles the shape of a separated drift, the progressive lateral coarsening of the material with increasing distance from the moat implies that the southern bank acted as the main source for coarse-grained material. We propose that the Kveithola Drift represents a combination of an off-bank wedge and a confined drift. Our findings suggest that seismo-acoustic data should be accompanied by grain-size measurements on sediment cores in order to gain a reliable interpretation of the forcing mechanism that shaped a sediment drift.

Acknowledgments

This study was funded through DFG-Research Center / Cluster of Excellence "The Ocean in the Earth System" (MARUM project SD2) and PNRA-CORIBAR-IT (2013/C2.01) and the ARCA project (grant n. 25_11_2013_973), in the frame of the joint CORIBAR consortium effort. We thank the scientific party of the CORIBAR cruise for their collaboration in sampling and analyzing the sediment cores. Special thanks go to captain Matthias Günther and his crew on RV Maria S. Merian for their outstanding support during research cruise MSM30 CORIBAR. We wish to thank Asli Özmaral for providing figures, Thomas Frederichs for his support with MSCL scanning, Brit Kockisch for her lab support, and Andre Hüpers for his help with the vane shear strength measurements. We also would like to thank the two anonymous reviewers for their very constructive comments. Interpretation of sediment echosounder data was done with the IHS Kingdom software. The data reported in this paper are archived in Pangaea (www.pangaea.de).

References

Andersen, E.S., Dokken, T.M., Elverhøi, A., Solheim, A., Fossen, I., 1996. Late quaternary sedimentation and glacial history of the western Svalbard continental margin. Marine Geology 133 (3–4), 123-156.

Andersen, C., Koç, N., Jennings, A., Andrews, J.T., 2004. Nonuniform response of the major surface currents in the Nordic Seas to insolation forcing: Implications for the Holocene climate variability. Paleoceanography 19 (2), PA2003.

Andreassen, K., Laberg, J.S., Vorren, T.O., 2008. Seafloor geomorphology of the SW Barents Sea and its glaci-dynamic implications. Geomorphology 97 (1–2), 157-177.

Batchelor, C.L., Dowdeswell, J.A., 2014. The physiography of High Arctic cross-shelf troughs. Quaternary Science Reviews 92, 68-96.

Bergh, S.G., Grogan, P., 2003. Tertiary structure of the Sørkapp-Hornsund Region, South Spitsbergen, and implications for the offshore southern extension of the fold-thrust belt. Norwegian Journal of Geology 83, 43-60.

Birks, C.J.A., Koç, N., 2002. A high-resolution diatom record of late-Quaternary sea-surface temperatures and oceanographic conditions from the eastern Norwegian Sea. Boreas 31 (4), 323-344.

Bjarnadóttir, L.R., Rüther, D.C., Winsborrow, M.C.M., Andreassen, K., 2013. Grounding-line dynamics during the last deglaciation of Kveithola, W Barents Sea, as revealed by seabed geomorphology and shallow seismic stratigraphy. Boreas 42 (1), 84-107.

Bjarnadóttir, L.R., Winsborrow, M.C.M., Andreassen, K., 2014. Deglaciation of the central Barents Sea. Quaternary Science Reviews 92, 208-226.

Bjørlykke, K., Bue, B., Elverhøi, A., 1978. Quaternary sediments in the northwestern part of the Barents Sea and their relation to the underlying Mesozoic bedrock. Sedimentology 25 (2), 227-246.

Blanpied, C., Bellaiche, G., 1981. Bioturbation on the Pelagian Platform: Ichnofacies variations as paleoclimatic indicator. Marine Geology 43 (3), M49-M57.

Blaume, F., 1992. Hochakkumulationsgebiete am norwegischen Kontinentalhang: Sedimentologische Abbilder Topographie-geführter Strömungsmuster. Berichte Sonderforschungsbereich 313, 36 (1-83).

Bøe, R., Skarðhamar, J., Rise, L., Dolan, M.F.J., Bellec, V.K., Winsborrow, M., Skagseth, Ø., Knies, J., King, E.L., Walderhaug, O., Chand, S., Buenz, S., Mienert, J., 2015. Sandwaves and sand transport on the Barents Sea continental slope offshore northern Norway. Marine and Petroleum Geology 60, 34-53.

Brendryen, J., Haflidason, H., Rise, L., Chand, S., Vanneste, M., Longva, O., L'Heureux, J.S., Forsberg, C.F., 2015. Ice sheet dynamics on the Lofoten–Vesterålen shelf, north Norway, from Late MIS-3 to Heinrich Stadial 1. Quaternary Science Reviews 119, 136-156.

Broecker, W.S., Denton, G.H., Edwards, R.L., Cheng, H., Alley, R.B., Putnam, A.E., 2010. Putting the Younger Dryas cold event into context. Quaternary Science Reviews 29 (9-10), 1078-1081.

Carbonara, K., Mezgec, K., Varagona, G., Musco, M.E., Lucchi, R.G., Villa, G., Morigi, C., Melis, R., Caffau, M., 2016. Palaeoclimatic changes in Kveithola, Svalbard, during the Late Pleistocene deglaciation and Holocene: Evidences from microfossil and sedimentary records. Palaeogeography, Palaeoclimatology, Palaeoecology 463, 136-149.

Cattaneo, A., Correggiari, A., Langone, L., Trincardi, F., 2003. The late-Holocene Gargano subaqueous delta, Adriatic shelf: sediment pathways and supply fluctuations. Marine Geology 193 (1-2), 61-91.

Cronin, T.M., 1999. Principles of Climatology. New York: Columbia University Press, p. 204.

Dowdeswell, J.A., Elverhfi, A., Spielhagen, R., 1998. Glaciomarine sedimentary processes and facies on the polar North Atlantic margins. Quaternary Science Reviews 17 (1–3), 243-272.

Dowdeswell, J.A., Cofaigh, C.Ó., Noormets, R., Larter, R.D., Hillenbrand, C.D., Benetti, S., Evans, J., Pudsey, C.J., 2008. A major trough-mouth fan on the continental margin of the Bellingshausen Sea, West Antarctica: The Belgica Fan. Marine Geology 252 (3–4), 129-140.

Ebbesen, H., Hald, M., Eplet, T.H., 2007. Lateglacial and early Holocene climatic oscillations on the western Svalbard margin, European Arctic. Quaternary Science Reviews 26 (15–16), 1999-2011.

Edwards, M.B., 1975. Gravel fraction on Spitsbergenbanken-NW Barents Sea. Norges Geologiske Undersøkelse 316, 205-217.

Elverhøi, A., Pfirman, S.L., Solheim, A., Larssen, B.B., 1989. Glaciomarine sedimentation in epicontinental seas exemplified by the northern Barents Sea. Marine Geology 85 (2–4), 225-250.

Elverhøi, A., Fjeldskaar, W., Solheim, A., Nyland-Berg, M., Russwurm, L., 1993. The Barents Sea Ice Sheet — A model of its growth and decay during the last ice maximum. Quaternary Science Reviews 12 (10), 863-873.

ElverhøI, A., Dowdeswell, J.A., Funder, S., Mangerud, J.A.N., Stein, R., 1998. Glacial and oceanic history of the polar North Atlantic margins: an overview. Quaternary Science Reviews 17 (1–3), 1-10.

Elverhøi, A., Andersen, E.S., Dokken, T., Hebbeln, D., Spielhagen, R., Svendsen, J.I., Sørflaten, M., Rørnes, A., Hald, M., Forsberg, C.F., 1995. The Growth and Decay of the Late Weichselian Ice Sheet in Western Svalbard and Adjacent Areas Based on Provenance Studies of Marine Sediments. Quaternary Research 44 (3), 303-316.

Elverhøi, A., Henrich, R., 2002. Past glaciomarine environments. In: Menzies, J. (Ed.) Modern and Past Glacial Environments. Butterworth-Heinemann, Oxford, pp. 391-415.

Faleide, J.I., Solheim, A., Fiedler, A., Hjelstuen, B.O., Andersen, E.S., Vanneste, K., 1996. Late Cenozoic evolution of the western Barents Sea-Svalbard continental margin. Global and Planetary Change 12 (1–4), 53-74.

Faugères, J.-C., Stow, D.A.V., Imbert, P., Viana, A., 1999. Seismic features diagnostic of contourite drifts. Marine Geology 162 (1), 1-38.

Faugères, J.C., Stow, D.A.V., 2008. Contourite drifts: nature, evolution and controls. In: Rebesco, M., Camerlenghi, A. (Eds.), Contourites - Developments in Sedimentology 60. pp. 259-288.

Fohrmann, H., 1996. Sedimente in bodengebundenen Dichteströmungen, Numerische Fallstudien. Beriche Sonderforschungsbereich 313, 66, 1-106.

Fohrmann, H., Backhaus, J.O., Blaume, F., Rumohr, J., 1998. Sediments in bottom-arrested gravity plumes: Numerical case studies. Journal of Physical Oceanography 28 (11), 2250-2274.

Forsberg, C.F., Solheim, A., Elverhøi, A., Jansen, E., Channell, J.E.T., Andersen, E.S., 1999. The depositional environment of the western Svalbard margin during the Late Pliocene and the Pleistocene: sedimentary facies changes at Site 986. In: Raymo, M.E., Jansen, E., Blum, P., Herbert, T.D. (Eds.), Proceedings of the Ocean Drilling Program, Scientific Results, Vol. 162.

Forwick, M., Vorren, T.O., 2009. Late Weichselian and Holocene sedimentary environments and ice rafting in Isfjorden, Spitsbergen. Palaeogeography, Palaeoclimatology, Palaeoecology 280 (1–2), 258-274.

Gabrielsen, R.H., Færseth, R.B., Jensen, L.N., Kalheim, J.E., Riis, F., 1990. Structural elements of the Norwegian continental shelf, part I: the Barents Sea region. Norwegian Petroleum Directorate Bulletin 6, 4-33.

Hald, M., Vorren, T.O., 1984. Modern and Holocene foraminifera and sediments on the continental shelf off Troms, North Norway. Boreas 13 (2), 133-154.

Hald, M., Andersson, C., Ebbesen, H., Jansen, E., Klitgaard-Kristensen, D., Risebrobakken, B., Salomonsen, G.R., Sarnthein, M., Sejrup, H.P., Telford, R.J., 2007. Variations in temperature and extent of Atlantic Water in the northern North Atlantic during the Holocene. Quaternary Science Reviews 26 (25–28), 3423-3440.

Hanebuth, T.J.J., Lantzsch, H., Bergenthal, M., Caburlotto, A., Dippold, S., Düßmann, R., Freudenthal, T., Hörner, T., Kaszemeik, K., Klar, S., Llopart, J., Lucchi, R.G., Nicolaisen, L.S., Noorlander, K., Osti, G., Özmaral, A., Rebesco, M., Rosiak, U., Sabbatini, A., Schmidt, W., Stachowski, A., Urgeles, R., 2013. CORIBAR – Ice dynamics and meltwater deposits: coring in the Kveithola Trough, NW Barents Sea. Cruise MSM30. 16.07. – 15.08.2013, Tromsø (Norway) – Tromsø (Norway). Berichte, MARUM – Zentrum für Marine Umweltwissenschaften, Fachbereich Geowissenschaften, Universität Bremen 299, 74 pp.

Hanebuth, T.J.J., Rebesco, M., Urgeles, R., Lucchi, R.G., Freudenthal, T., 2014. Drilling Glacial Deposits in Offshore Polar Regions. Eos, Transactions American Geophysical Union 95 (31), 277-278.

Hanebuth, T.J.J., Zhang, W., Hofmann, A.L., Löwemark, L.A., Schwenk, T., 2015. Oceanic density fronts steering bottom-current induced sedimentation deduced from a 50 ka contourite-drift record and numerical modeling (off NW Spain). Quaternary Science Reviews 112, 207-225.

Henrich, R., Freiwald, A., Bickert, T., Schäfer, P., 1997. Evolution of an Arctic Open-Shelf Carbonate Platform, Spitsbergen Bank (Barents Sea)Cool-Water Carbonates. SEPM Society for Sedimentary Geology, pp. 163-181.

Hesse, R., Khodabakhsh, S., Klaucke, I., Ryan, W.B.F., 1997. Asymmetrical turbid surface-plume deposition near ice-outlets of the Pleistocene Laurentide ice sheet in the Labrador Sea. Geo-Marine Letters 17 (3), 179-187.

Jakobsson, M., Mayer, L., Coakley, B., Dowdeswell, J.A., Forbes, S., Fridman, B., Hodnesdal, H., Noormets, R., Pedersen, R., Rebesco, M., Schenke, H.W., Zarayskaya, Y., Accettella, D., Armstrong, A., Anderson, R.M., Bienhoff, P., Camerlenghi, A., Church, I., Edwards, M., Gardner, J.V., Hall, J.K., Hell, B., Hestvik, O., Kristoffersen, Y., Marcussen, C., Mohammad, R., Mosher, D., Nghiem, S.V., Pedrosa, M.T., Travaglini, P.G., Weatherall, P., 2012. The International Bathymetric Chart of the Arctic Ocean (IBCAO) Version 3.0. Geophysical Research Letters 39 (12), L12609.

Jessen, S.P., Rasmussen, T.L., Nielsen, T., Solheim, A., 2010. A new Late Weichselian and Holocene marine chronology for the western Svalbard slope 30,000–0 cal years BP. Quaternary Science Reviews 29 (9–10), 1301-1312.

Johnson, H.D., Baldwin, C.T., 1996. Shallow clastic seas. In: Reading, H.G. (Ed.) Sedimentary environments: processes, facies and stratigraphy. Blackwell, Malden, Oxford, Carlton, pp. 232-280.

Johnsen, S.J., Dahl-Jensen, D., Gundestrup, N., Steffensen, J.P., Clausen, H.B., Miller, H., Masson-Delmotte, V., Sveinbjörnsdottir, A.E., White, J., 2001. Oxygen isotope and palaeotemperature records from six Greenland ice-core stations: Camp Century, Dye-3, GRIP, GISP2, Renland and NorthGRIP. Journal of Quaternary Science 16 (4), 299-307.

King, E.L., Bøe, R., Bellec, V.K., Rise, L., Skarðhamar, J., Ferré, B., Dolan, M.F.J., 2014. Contour current driven continental slope-situated sandwaves with effects from secondary current processes on the Barents Sea margin offshore Norway. Marine Geology 353, 108-127.

Koç, N., Jansen, E., Haflidason, H., 1993. Paleoceanographic reconstructions of surface ocean conditions in the Greenland, Iceland and Norwegian seas through the last 14 ka based on diatoms. Quaternary Science Reviews 12 (2), 115-140.

Laberg, J.S., Vorren, T.O., 1995. Late Weichselian submarine debris flow deposits on the Bear Island Trough Mouth Fan. Marine Geology 127 (1–4), 45-72.

Landvik, J.Y., Bondevik, S., ElverhØI, A., Fjeldskaar, W., Mangerud, J.A.N., Salvigsen, O., Siegert, M.J., Svendsen, J.-I., Vorren, T.O., 1998. The Last Glacial Maximum of Svalbard and the Barents Sea area: ice sheet extent and configuration. Quaternary Science Reviews 17 (1–3), 43-75.

Llopart, J., Urgeles, R., Camerlenghi, A., Lucchi, R.G., De Mol, B., Rebesco, M., Pedrosa, M.T., 2014. Slope Instability of Glaciated Continental Margins: Constraints from Permeability-Compressibility Tests and Hydrogeological Modeling Off Storfjorden, NW Barents Sea. In: Krastel, S., Behrmann, J.-H., Völker, D., Stipp, M., Berndt, C., Urgeles, R., Chaytor, J., Huhn, K., Strasser, M., Harbitz, C.B. (Eds.), Submarine Mass Movements and Their Consequences: 6th International Symposium. Springer International Publishing, Cham, pp. 95-104.

Llopart, J., Urgeles, R., Camerlenghi, A., Lucchi, R.G., Rebesco, M., De Mol, B., 2015. Late Quaternary development of the Storfjorden and Kveithola Trough Mouth Fans, northwestern Barents Sea. Quaternary Science Reviews 129, 68-84.

Loeng, H., 1991. Features of the physical oceanographic conditions of the Barents Sea. Polar Research 10 (1), 5-18.

Lucchi, R.G., Pedrosa, M.T., Camerlenghi, A., Urgeles, R., De Mol, B., Rebesco, M., 2012. Recent Submarine Landslides on the Continental Slope of Storfjorden and Kveithola Trough-Mouth Fans (North West Barents Sea). In: Yamada, Y., Kawamura, K., Ikehara, K., Ogawa, Y., Urgeles, R., Mosher, D., Chaytor, J., Strasser, M. (Eds.), Submarine Mass Movements and Their Consequences: 5th International Symposium. Springer Netherlands, Dordrecht, pp. 735-745.

Lucchi, R.G., Camerlenghi, A., Rebesco, M., Colmenero-Hidalgo, E., Sierro, F.J., Sagnotti, L., Urgeles, R., Melis, R., Morigi, C., Bárcena, M.A., Giorgetti, G., Villa, G., Persico, D., Flores, J.A., Rigual-Hernández, A.S., Pedrosa, M.T., Macri, P., Caburlotto, A., 2013. Postglacial sedimentary processes on the Storfjorden and Kveithola trough mouth fans: Significance of extreme glacimarine sedimentation. Global and Planetary Change 111, 309-326.

Lucchi, R.G., Sagnotti, L., Camerlenghi, A., Macrì, P., Rebesco, M., Pedrosa, M.T., Giorgetti, G., 2015. Marine sedimentary record of Meltwater Pulse 1a along the NW Barents Sea continental margin. Arktos 1 (1), 1-14.

Mangerud, J., Bondevik, S., Gulliksen, S., Karin Hufthammer, A., Høisæter, T., 2006. Marine 14C reservoir ages for 19th century whales and molluscs from the North Atlantic. Quaternary Science Reviews 25 (23–24), 3228-3245.

Mangerud, J.A.N., Landvik, J.Y., 2007. Younger Dryas cirque glaciers in western Spitsbergen: smaller than during the Little Ice Age. Boreas 36 (3), 278-285.

McCave, I.N., Manighetti, B., Robinson, S.G., 1995. Sortable silt and fine sediment size/composition slicing: Parameters for palaeocurrent speed and palaeoceanography. Paleoceanography 10 (3), 593-610.

Newton, A.M.W., Huuse, M., 2017. Glacial geomorphology of the central Barents Sea: Implications for the dynamic deglaciation of the Barents Sea Ice Sheet. Marine Geology 387, 114-131.

Ó Cofaigh, C., Stokes, C.R., 2008. Reconstructing ice-sheet dynamics from subglacial sediments and landforms: introduction and overview. Earth Surface Processes and Landforms 33, 495–502.

Ottesen, D., Dowdeswell, J.A., Rise, L., Rokoengen, K., Henriksen, S., 2002. Large-scale morphological evidence for past ice-stream flow on the mid-Norwegian continental margin. Geological Society, London, Special Publications 203 (1), 245-258.

Patton, H., Hubbard, A., Andreassen, K., Winsborrow, M., Stroeven, A.P., 2016. The build-up, configuration, and dynamical sensitivity of the Eurasian ice-sheet complex to Late Weichselian climatic and oceanic forcing. Quaternary Science Reviews 153, 97-121.

Patton, H., Andreassen, K., Bjarnadóttir, L.R., Dowdeswell, J.A., Winsborrow, M.C.M., Noormets, R., Polyak, L., Auriac, A., Hubbard, A., 2015. Geophysical constraints on the dynamics and retreat of the Barents Sea ice sheet as a paleobenchmark for models of marine ice sheet deglaciation. Reviews of Geophysics 53 (4), 1051-1098.

Preu, B., Hernández-Molina, F.J., Violante, R., Piola, A.R., Paterlini, C.M., Schwenk, T., Voigt, I., Krastel, S., Spiess, V., 2013. Morphosedimentary and hydrographic features of the northern Argentine margin: The interplay between erosive, depositional and gravitational processes and its conceptual implications. Deep Sea Research Part I: Oceanographic Research Papers 75 (0), 157-174.

Rasmussen, T.L., Thomsen, E., Ślubowska, M.A., Jessen, S., Solheim, A., Koç, N., 2007. Paleoceanographic evolution of the SW Svalbard margin (76°N) since 20,000 14C yr BP. Quaternary Research 67 (1), 100-114.

Rebesco, M., Stow, D., 2001. Seismic expression of contourites and related deposits: a preface. Marine Geophysical Researches 22 (5), 303-308.

Rebesco, M., Camerlenghi, A., 2008. Contourites - Developments in Sedimentology 60. p. 663.

Rebesco, M., Liu, Y., Camerlenghi, A., Winsborrow, M., Laberg, J.S., Caburlotto, A., Diviacco, P., Accettella, D., Sauli, C., Wardell, N., Tomini, I., 2011. Deglaciation of the western margin of the Barents Sea Ice Sheet — A swath bathymetric and sub-bottom seismic study from the Kveithola Trough. Marine Geology 279 (1–4), 141-147.

Rebesco, M., Laberg, J.S., Pedrosa, M.T., Camerlenghi, A., Lucchi, R.G., Zgur, F., Wardell, N., 2014a. Onset and growth of Trough-Mouth Fans on the North-Western Barents Sea margin – implications for the evolution of the Barents Sea/Svalbard Ice Sheet. Quaternary Science Reviews 92, 227-234.

Rebesco, M., Hernández-Molina, F.J., Van Rooij, D., Wåhlin, A., 2014b. Contourites and associated sediments controlled by deep-water circulation processes: State-of-the-art and future considerations. Marine Geology 352, 111-154.

Rebesco, M., Özmaral, A., Urgeles, R., Accettella, D., Lucchi, R.G., Rüther, D., Winsborrow, M., Llopart, J., Caburlotto, A., Lantzsch, H., Hanebuth, T.J.J., 2016a. Evolution of a high-latitude sediment drift inside a glacially-carved trough based on high-resolution seismic stratigraphy (Kveithola, NW Barents Sea). Quaternary Science Reviews 147, 178-193.

Rebesco, M., Urgeles, R., Özmaral, A., and the CORIBAR Scientific Party, 2016b. Grounding-zone wedges and mega-scale glacial lineations in Kveithola Trough, Barents Sea. Geological Society, London, Memoirs 46 (1), 231-232.

Reimer, P.J., Bard, E., Bayliss, A., Beck, J.W., Blackwell, P.G., Ramsey, C.B., Buck, C.E., Cheng, H., Edwards, R.L., Friedrich, M., Grootes, P.M., Guilderson, T.P., Haflidason, H., Hajdas, I., Hatté, C., Heaton, T.J., Hoffmann, D.L., Hogg, A.G., Hughen, K.A., Kaiser, K.F., Kromer, B., Manning, S.W., Niu, M., Reimer, R.W., Richards, D.A., Scott, E.M., Southon, J.R., Staff, R.A., Turney, C.S.M., van der Plicht, J., 2013. IntCal13 and Marine13 Radiocarbon Age Calibration Curves 0–50,000 Years cal BP. Radiocarbon 55 (04), 1869-1887.

Rigual-Hernández, A.S., Colmenero-Hidalgo, E., Martrat, B., Bárcena, M.A., de Vernal, A., Sierro, F.J., Flores, J.A., Grimalt, J.O., Henry, M., Lucchi, R.G., 2017. Svalbard ice-sheet decay after the Last Glacial Maximum: New insights from micropalaeontological and organic biomarker paleoceanographical reconstructions. Palaeogeography, Palaeoclimatology, Palaeoecology 465, Part A, 225-236.

Rüther, D.C., Mattingsdal, R., Andreassen, K., Forwick, M., Husum, K., 2011. Seismic architecture and sedimentology of a major grounding zone system deposited by the Bjørnøyrenna Ice Stream during Late Weichselian deglaciation. Quaternary Science Reviews 30 (19–20), 2776-2792.

Rüther, D.C., Bjarnadóttir, L.R., Junttila, J., Husum, K., Rasmussen, T.L., Lucchi, R.G., Andreassen, K., 2012. Pattern and timing of the northwestern Barents Sea Ice Sheet deglaciation and indications of episodic Holocene deposition. Boreas 41 (3), 494-512.

Sættem, J., Poole, D.A.R., Ellingsen, L., Sejrup, H.P., 1992. Glacial geology of outer Bjørnøyrenna, southwestern Barents Sea. Marine Geology 103 (1), 15-51.

Sarnthein, M., Van Kreveld, S., Erlenkeuser, H., Grootes, P.M., Kucera, M., Pflaumann, U., Schulz, M., 2003. Centennial-to-millennial-scale periodicities of Holocene climate and sediment injections off the western Barents shelf, 75°N. Boreas 32 (3), 447-461.

Siegert, M.J., Dowdeswell, J.A., 2002. Late Weichselian iceberg, surface-melt and sediment production from the Eurasian Ice Sheet: results from numerical ice-sheet modelling. Marine Geology 188 (1–2), 109-127.

Ślubowska-Woldengen, M., Rasmussen, T.L., Koç, N., Klitgaard-Kristensen, D., Nilsen, F., Solheim, A., 2007. Advection of Atlantic Water to the western and northern Svalbard shelf since 17,500 cal yr BP. Quaternary Science Reviews 26 (3–4), 463-478.

Ślubowska-Woldengen, M., Koç, N., Rasmussen, T.L., Klitgaard-Kristensen, D., Hald, M., Jennings, A.E., 2008. Time-slice reconstructions of ocean circulation changes on the continental shelf in the Nordic and Barents Seas during the last 16,000 cal yr B.P. Quaternary Science Reviews 27 (15–16), 1476-1492.

Stiansen, J.E., Filin, A.A., 2007. Joint PINRO/IMR Report on the State of the Barents Sea Ecosystem 2006, with Expected Situation and Considerations for Management, IMR/PINRO Joint Report Series No. 2. p. 209.

Stokes, C.R., Clark, C.D., 1999. Geomorphological criteria for identifying Pleistocene ice streams. Annals of Glaciology 28 (1), 67-74.

Stow, D.A.V., Faugères, J.-C., Howe, J.A., Pudsey, C.J., Viana, A.R., 2002. Bottom currents, contourites and deep-sea sediment drifts: current state-of-the-art. Geological Society, London, Memoirs 22 (1), 7-20.

Stuiver, M., Reimer, P.J., Bard, E., Beck, J.W., Burr, G.S., Hughen, K.A., Kromer, B., McCormac, G., Van der Plicht, J., Spurk, M., 1998. INTCAL98 radiocarbon age calibration, 24,000–0 cal BP. Radiocarbon 40 (3), 1041-1083.

Svendsen, J.I., Mangerud, J., 1992. Paleoclimatic inferences from glacial fluctuations on Svalbard during the last 20 000 years. Climate Dynamics 6, 213-220.

Svendsen, J.I., Elverhøi, A., Mangerud, J., 1996. The retreat of the Barents Sea Ice Sheet on the western Svalbard margin. Boreas 25 (4), 244-256.

Swift, J.H., 1986. The Arctic waters. In: Hurdle, G.B. (Ed.) The Nordic Seas. Springer, New York Inc., pp. 129–153.

Swift, D.J.P., Thorne, J.A., 1991. Sedimentation on continental margins, I: a general model for shelf sedimentation. In: Swift, D.J.P., Oertel, G.F., Tillman, R.W., Thorne, J.A. (Eds.), Shelf sand and sandstone bodies, geometry, facies and sequence stratigraphy - International Association of Sedimentologists Special Publication 14. Blackwell, Oxford, pp. 3-31.

Telford, R.J., Heegaard, E., Birks, H.J.B., 2004. The intercept is a poor estimate of a calibrated radiocarbon age. The Holocene 14 (2), 296-298.

Verdicchio, G., Trincardi, F., 2006. Short-distance variability in slope bed-forms along the Southwestern Adriatic Margin (Central Mediterranean). Marine Geology 234 (1–4), 271-292.

Verdicchio, G., Trincardi, F., 2008a. Shallow-water contourites. In: Rebesco, M., Camerlenghi, A. (Eds.), Contourites - Developments in Sedimentology 60. Elsevier, Amsterdam, Oxford, pp. 409-433.

Verdicchio, G., Trincardi, F., 2008b. Mediterranean shelf-edge muddy contourites: examples from the Gela and South Adriatic basins. Geo-Marine Letters 28 (3), 137-151.

Viana, A.R., Faugères, J.-C., 1998. Upper slope sand deposits: the example of Campos Basin, a latest Pleistocene-Holocene record of the interaction between alongslope and downslope currents. Geological Society, London, Special Publications 129 (1), 287-316.

Viana, A.R., 2001. Seismic expression of shallow- to deep-water contourites along the south-eastern Brazilian margin. Marine Geophysical Researches 22 (5-6), 509-521.

Voigt, I., Henrich, R., Preu, B.M., Piola, A.R., Hanebuth, T.J.J., Schwenk, T., Chiessi, C.M., 2013. A submarine canyon as a climate archive — Interaction of the Antarctic Intermediate Water with the Mar del Plata Canyon (Southwest Atlantic). Marine Geology 341 (0), 46-57.

Vorren, T.O., Strass, I.F., Lind-Hansen, O.W., 1978. Late Quaternary sediments and stratigraphy on the continental shelf off Troms and west Finnmark, northern Norway. Quaternary Research 10 (3), 340-365.

Vorren, T.O., Hald, M., Thomsen, E., 1984. Sedimentation on High-latitude Continental Shelves Quaternary sediments and environments on the continental shelf off northern Norway. Marine Geology 57 (1), 229-257.

Vorren, T.O., Laberg, J.S., 1996. Late glacial air temperature, oceanographic and ice sheet interactions in the southern Barents Sea region. In: Andrews, J.T., Austin, W.E.N., Bergsten, H., Jennings, A.E. (Eds.), Late Quaternary Palaeoceanography of the North Atlantic Margins. pp. 303-321.

Walker, M.J.C., Berkelhammer, M., Björck, S., Cwynar, L.C., Fisher, D.A., Long, A.J., Lowe, J.J., Newnham, R.M., Rasmussen, S.O., Weiss, H., 2012. Formal subdivision of the Holocene Series/Epoch: a Discussion Paper by a Working Group of INTIMATE (Integration of ice-core, marine and terrestrial records) and the Subcommission on Quaternary Stratigraphy (International Commission on Stratigraphy). Journal of Quaternary Science 27 (7), 649-659.

Winsborrow, M.C.M., Andreassen, K., Corner, G.D., Laberg, J.S., 2010. Deglaciation of a marine-based ice sheet: Late Weichselian palaeo-ice dynamics and retreat in the southern Barents Sea reconstructed from onshore and offshore glacial geomorphology. Quaternary Science Reviews 29 (3–4), 424-442.

Zaborska, A., Carroll, J., Papucci, C., Torricelli, L., Carroll, M.L., Walkusz-Miotk, J., Pempkowiak, J., 2008. Recent sediment accumulation rates for the Western margin of the Barents Sea. Deep Sea Research Part II: Topical Studies in Oceanography 55 (20–21), 2352-2360.

Zecchin, M., Rebesco, M., Lucchi, R.G., Caffau, M., Lantzsch, H., Hanebuth, T.J.J., 2016. Buried iceberg-keel scouring on the southern Spitsbergenbanken, NW Barents Sea. Marine Geology 382, 68-79.

Figure captions

Fig. 1: Map of the study area showing bathymetry, acoustic profiles, and sediment core locations (modified from Rebesco et al., 2016a). Bathymetric data was combined using new data from the CORIBAR cruise, pre-existing multibeam datasets (Rüther et al., 2012; Bjarnadóttir et al., 2013) and IBCAO data (Jakobsson et al., 2012). Grid size: 20 m for water depths shallower than 700 m, 40 m in deeper areas; vertical exaggeration: 2.7. Acoustic profiles presented in this study are displayed as white lines, sediment coring sites are shown as black dots. A dashed dark gray line indicates the outline of the Kveithola Drift. Inlay map shows the location of the study area between Bear Island and Svalbard (red box) as well as modern oceanographic circulation pattern after Loeng (1991) and Stiansen and Filin (2007): red arrows - Atlantic Water; blue arrows - Arctic Water; black line - mean position of the Polar Front.

Fig. 2: Sediment-acoustic profile on Spitsbergenbanken south of the Kveithola Trough (see Fig. 1 for location) and interpretation of the stratigraphic architecture. B6–B1: main stratigraphic units. Note that B1 and B2 are superimposed by the high-amplitude seafloor reflection. Black arrows indicate sediment core locations (see Fig. 3 for respective sediment core columns). The weak, westward dipping reflector in the overview profile represents an internal reflection surface within B6.

Fig. 3: Logs of sediment cores from Spitsbergenbanken (see Figs. 1 and 2 for location) displaying lithology, magnetic susceptibility, grain size of mud and sand fractions, carbonate content, and radiocarbon ages. Interpretation of acoustic profiles, core lithology, and radiocarbon dates allowed to correlate the stratigraphic units B6 to B1. Dashed unit boundaries indicate a less robust age control than solid lines (see chapter 5.2).

Fig. 4: Representative radiographic images of sedimentary facies types: (A) B5 showing fine lamination without bioturbation (core GeoB17629-2, 420-445 cm); (B) crudely laminated B4 with dispersed mm-to cm-sized lithic fragments (GeoB17631-2, 279-304 cm); (C) B3 containing abundant lithic particles and carbonate shell fragments, and some pyritized micro-burrows “Mycellia” (*sensu* Blanpied and Bellaiche, 1981; GeoB17631-2, 254-279 cm); (D) B3 with less lithic and carbonate fragments but abundant pyritized micro-burrows (GeoB17631-2, 178-203 cm). Denser material is displayed in darker tones. Note that the sediment might have bent down at its margin during vibrocoring.

Fig. 5: Sediment-acoustic profile inside the Kveithola Trough (see Fig. 1 for location) and interpretation of the stratigraphic architecture. T6–T1: main stratigraphic units. Black arrows indicate sediment core locations (see Fig. 7 for sediment core logs).

Fig. 6: Sediment-acoustic profile of the Kveithola Trough (see Fig. 1 for location) and interpretation of the stratigraphic architecture. T6–T1: main stratigraphic units. Black arrows indicate sediment core locations (see Fig. 8 for sediment core logs).

Fig. 7: Logs of sediment cores from the Kveithola Trough (see Figs. 1 and 5 for location) displaying magnetic susceptibility, grain size, and radiocarbon ages. The ratio Ca/Fe indicates terrigenous supply versus marine biogenous carbonate content. Al/Zr is used as a grain-size proxy displaying finer sediments to the right. Interpretation of acoustic profiles, core lithology and radiocarbon measurements allowed to correlate the stratigraphic units T4 to T1. Dashed unit boundaries indicate a less robust age control than solid lines (see chapter 5.2).

Fig. 8 Logs of sediment cores from the Kveithola Trough (see Figs. 1 and 6 for location) displaying magnetic susceptibility, grain size, and radiocarbon ages. The ratio Ca/Fe indicates terrigenous supply versus marine biogenous carbonate content. Al/Zr is used as an additional grain-size proxy displaying finer sediments to the right. Interpretation of acoustic profiles, core lithology and radiocarbon measurements allowed to correlate the stratigraphic units T5 to T1. Dashed unit boundaries indicate a less robust age control than solid lines (see chapter 5.2).

Fig. 9: Measured grain-size distribution data, exemplarily displayed by the grain-size variations in sediment core 17614-2 for sample depths 750 cm (Unit T4), 590 cm (T3), 410 cm (T2), and 250 cm (T1). Gray bars indicate the three main grain-size modes at 6-8, 20-25, and 50-105 µm.

Fig. 10: Compilation of radiocarbon ages from the study area and correlation of our stratigraphic units to the units of Rüther et al. (2012) and Rebesco et al. (2016a). Table 3 provides further information on all displayed radiocarbon ages. Dashed unit boundaries indicate a less robust age control than solid lines.

Fig. 11: Correlation of bank and trough stratigraphy and comparison to the stratigraphic interpretation by Rebesco et al. (2016a) and Rüther et al. (2012). Cores 17629-2 and 17614-2 exemplarily represent the stratigraphy of

Spitsbergenbanken and Kveithola Trough, respectively. Dashed unit boundaries indicate a less robust age control than solid lines.

Fig. 12: Correlation of the systems-wide environmental trends (exemplarily displayed by the grain-size variations in core 17614-2) with previous studies. References, core numbers, and type of proxy are provided in the header of the respective curves. The benthic foraminifer species *Cassidulina reniforme* and *Elphidium excavatum* display exemplarily the strength of Atlantic Water (AW) inflow into the eastern Nordic Seas continental shelf (Ślubowska-Woldengen et al., 2008). Strong Atlantic Water flow is indicated by a high abundance of *C. reniforme* and low percentages of *E. excavatum*. Grey bars indicate four time intervals emphasized by Ślubowska-Woldengen et al. (2008) stating the strength of Atlantic Water inflow.

Fig. 13: Different conceptual types of contourite drifts in terms of general geometry, grain-size distribution, sedimentation rates, and inferred bottom-current pathways. A-C are modified from: Faugères et al. (1999), Rebesco and Stow (2001), Stow et al., (2002); D and E illustrate the current pathways shaping the Kveithola Drift (AW = Atlantic Water; BSW = brine-enriched shelf waters).

Table captions

Table 1: Location of sediment cores and surface samples investigated in this study.

° from Rebesco et al. (2016a)

* from Rüther et al. (2012)

a Coring device: MUC = multicorer; GBC = giant box corer; GC = gravity corer; VC = vibrocorer.

Table 2: Results from vane shear strength measurements.

Table 3: Accelerator mass spectrometry (AMS) radiocarbon dates and calibrated ages.

a Radiocarbon laboratory: Poz = Poznań Radiocarbon Laboratory (Poland); TRa = Ångström Laboratory Uppsala (Norway).

b Material: bv = bivalves; pF = planktic foraminifers; bF = benthic foraminifers.

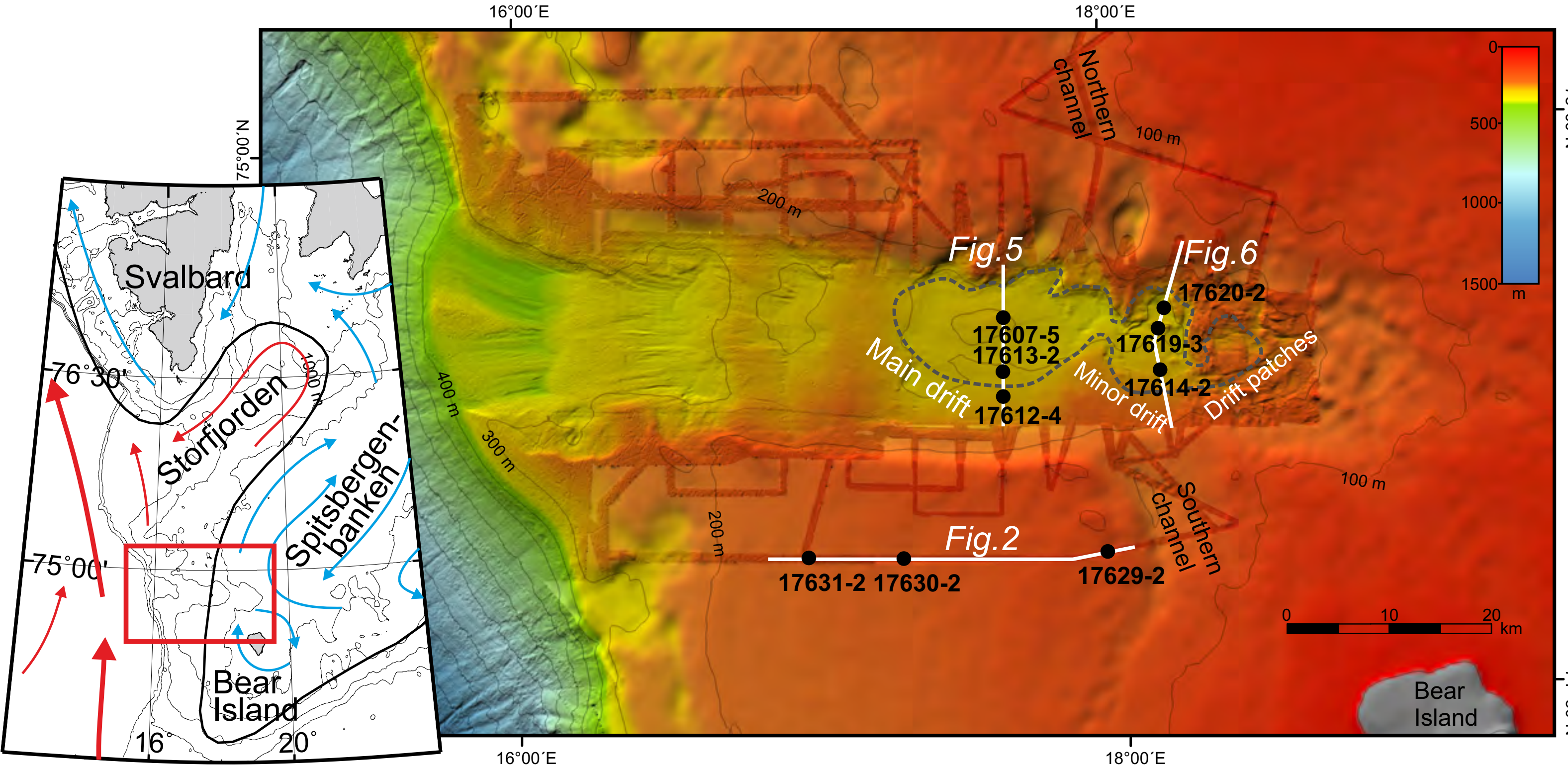

Svalbard
76°30'
Storfjorden
Spitsbergen-banken
75°00'
Bear Island
16°
20°
16°00´E
18°00´E
75°00´N
74° 30´N
Northern channel
100 m
200 m
400 m
300 m
Fig.5
Fig.6
17607-5
17613-2
17612-4
17620-2
17619-3
17614-2
Main drift
Minor drift
Drift patches
Fig.2
17631-2
17630-2
17629-2
Southern channel
0
10
20
km
500
1000
1500
m
Bear Island

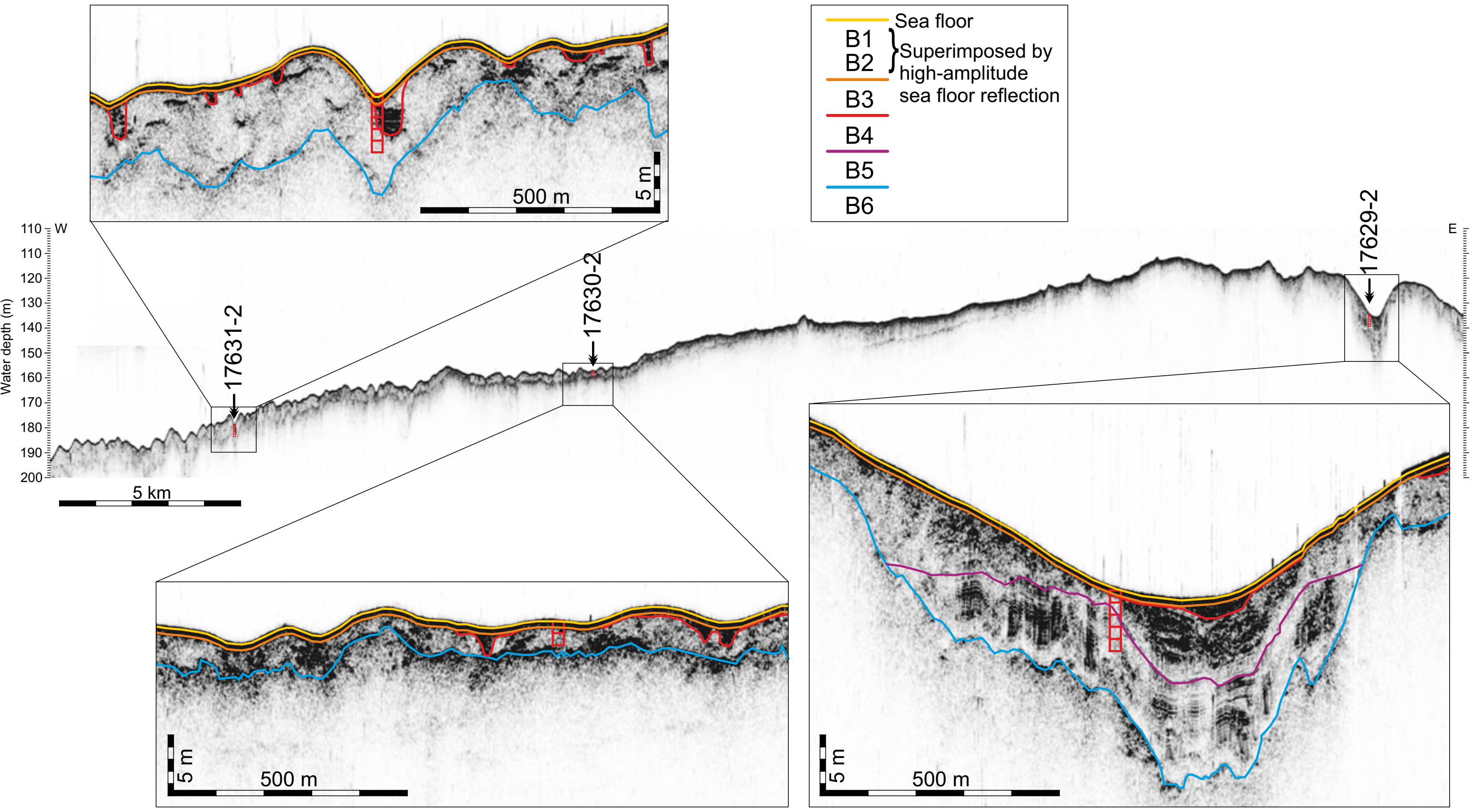
Sea floor
B1
B2
Superimposed by high-amplitude sea floor reflection
B3
B4
B5
B6
W
E
Water depth (m)
17631-2
17630-2
17629-2
5 km
500 m
5 m

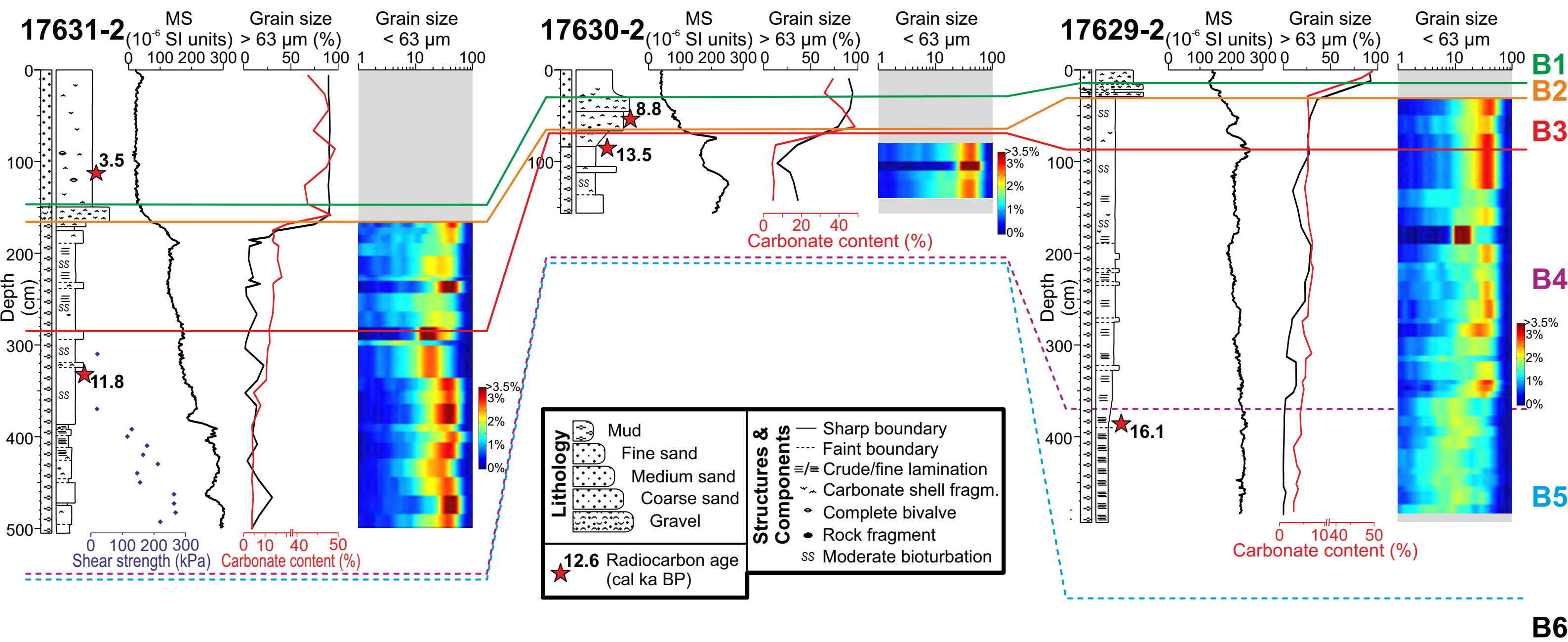

17631-2
17630-2
17629-2
MS (10⁻⁶ SI units)
Grain size > 63 µm (%)
Grain size < 63 µm
Depth (cm)
Shear strength (kPa)
Carbonate content (%)
3.5
11.8
8.8
13.5
16.1
B1
B2
B3
B4
B5
B6
Lithology
Mud
Fine sand
Medium sand
Coarse sand
Gravel
12.6 Radiocarbon age (cal ka BP)
Structures & Components
Sharp boundary
Faint boundary
Crude/fine lamination
Carbonate shell fragm.
Complete bivalve
Rock fragment
Moderate bioturbation

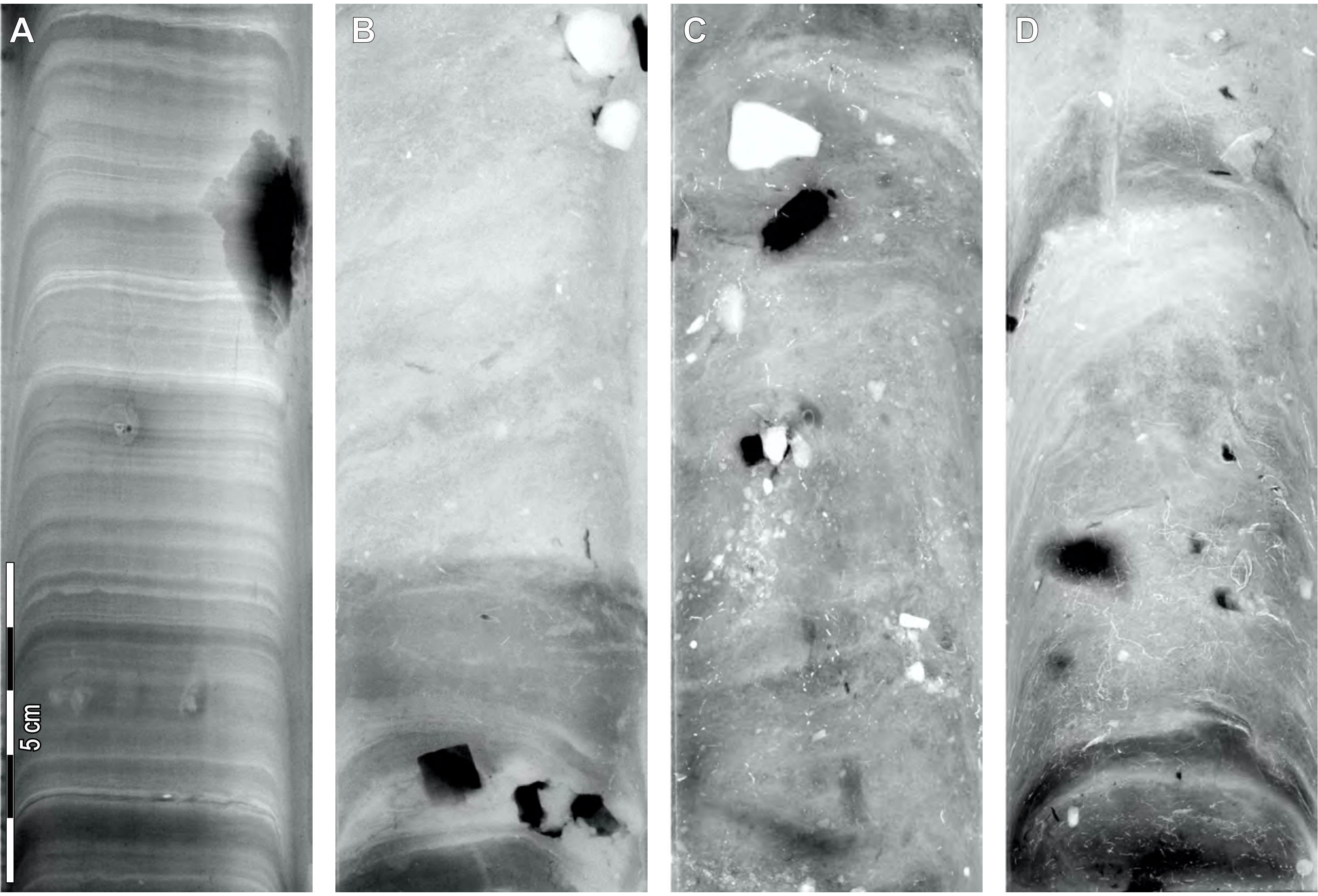
A
B
C
D
5 cm

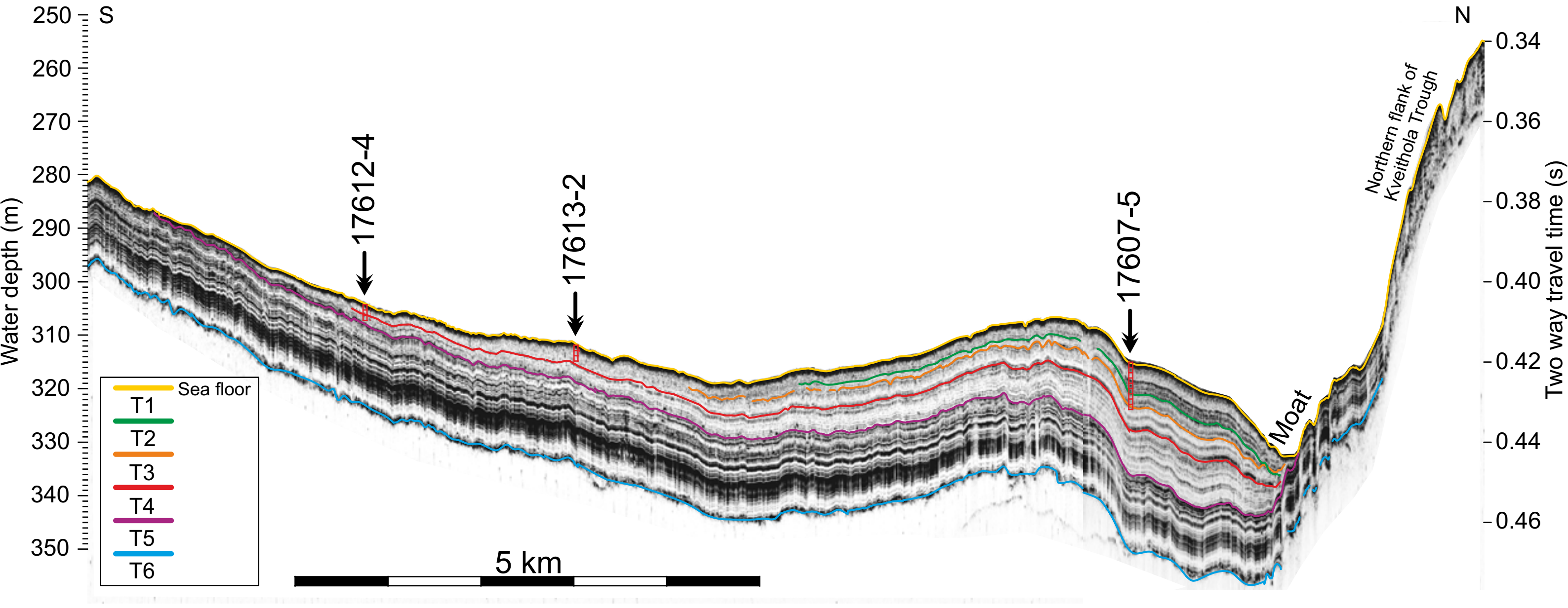

S
N
Water depth (m)
250
260
270
280
290
300
310
320
330
340
350
Two way travel time (s)
0.34
0.36
0.38
0.40
0.42
0.44
0.46
17612-4
17613-2
17607-5
Northern flank of Kveithola Trough
Moat
Sea floor
T1
T2
T3
T4
T5
T6
5 km

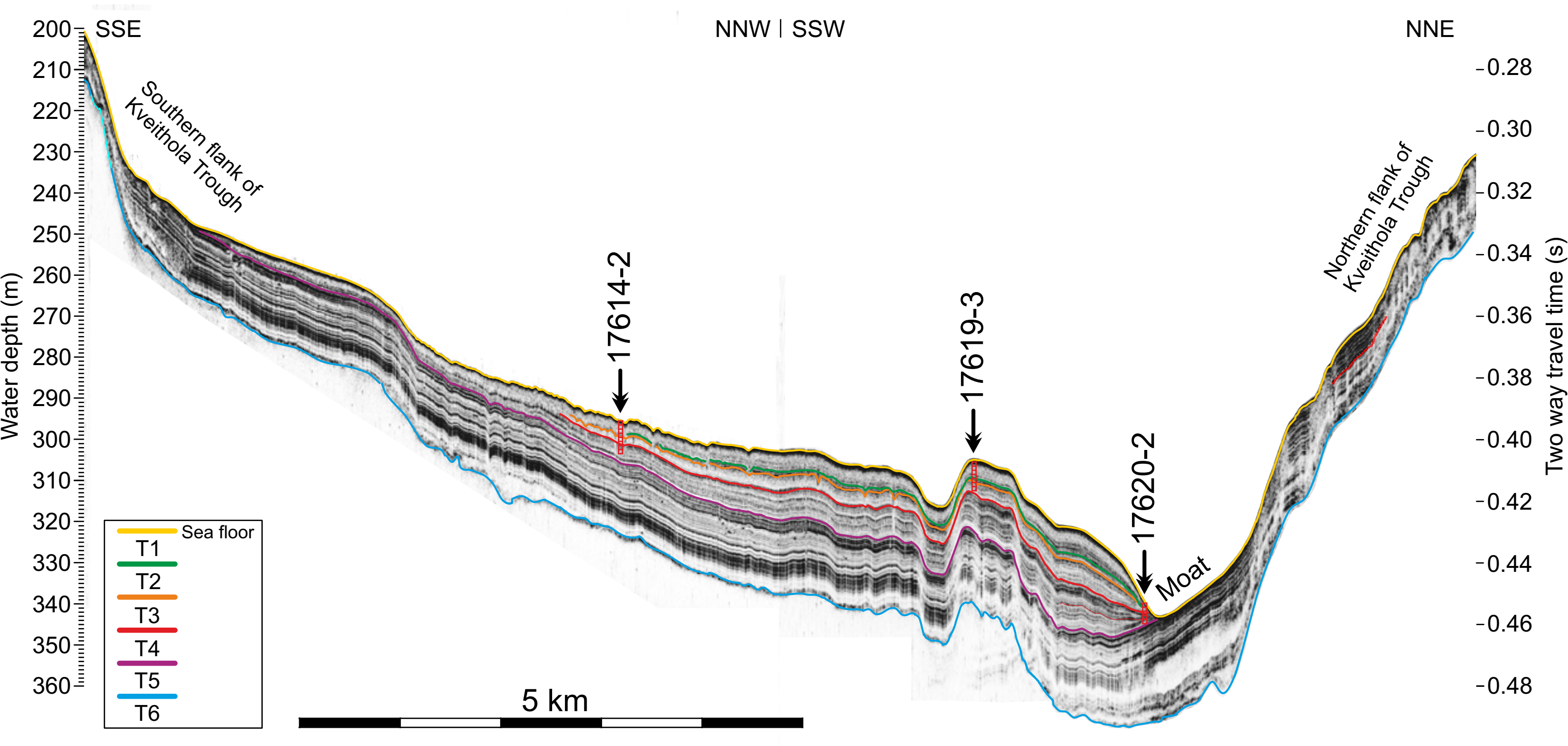

SSE
NNW | SSW
NNE
Southern flank of Kveithola Trough
Northern flank of Kveithola Trough
17614-2
17619-3
17620-2
Moat
Water depth (m)
Two way travel time (s)
200
210
220
230
240
250
260
270
280
290
300
310
320
330
340
350
360
-0.28
-0.30
-0.32
-0.34
-0.36
-0.38
-0.40
-0.42
-0.44
-0.46
-0.48
Sea floor
T1
T2
T3
T4
T5
T6
5 km

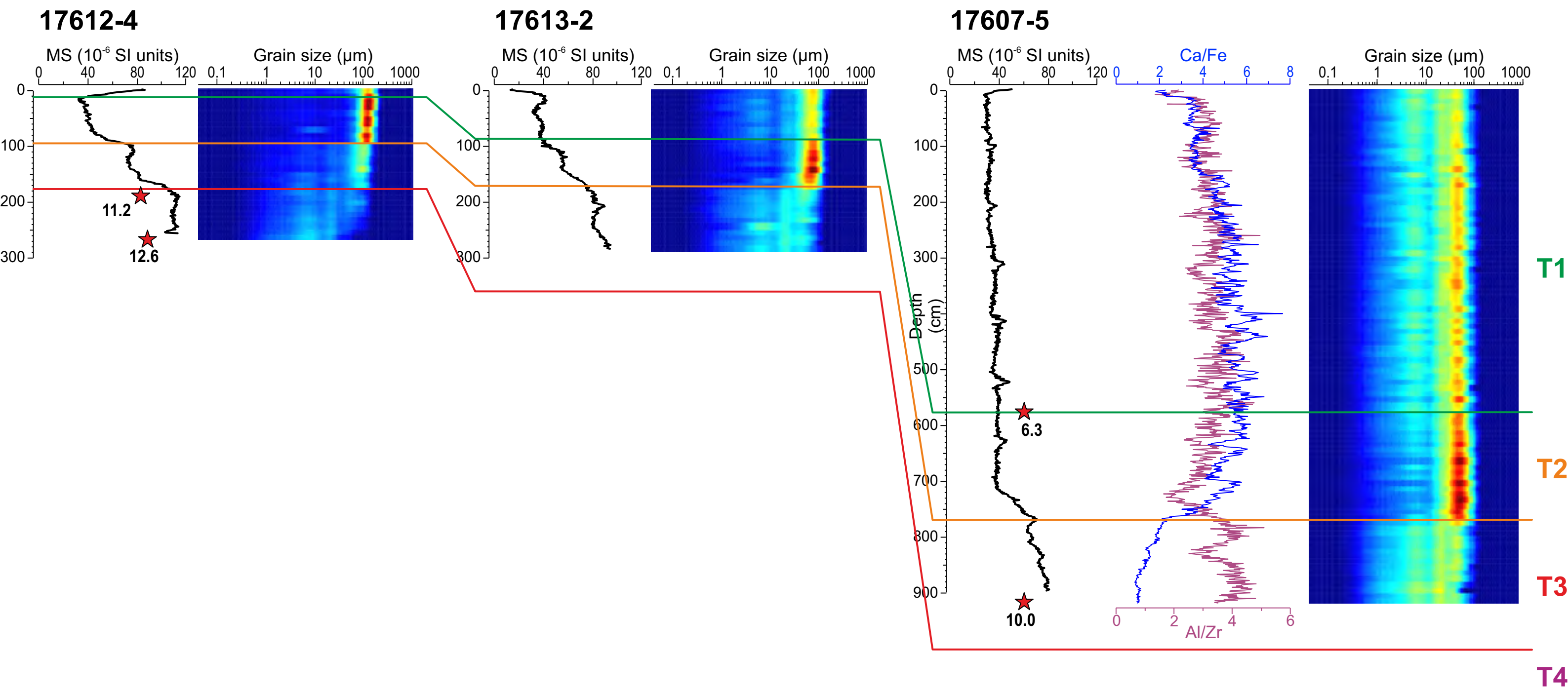

17612-4
MS (10-6 SI units)
Grain size (µm)
11.2
12.6
17613-2
MS (10-6 SI units)
Grain size (µm)
17607-5
MS (10-6 SI units)
Ca/Fe
Grain size (µm)
Depth (cm)
6.3
10.0
Al/Zr
T1
T2
T3
T4

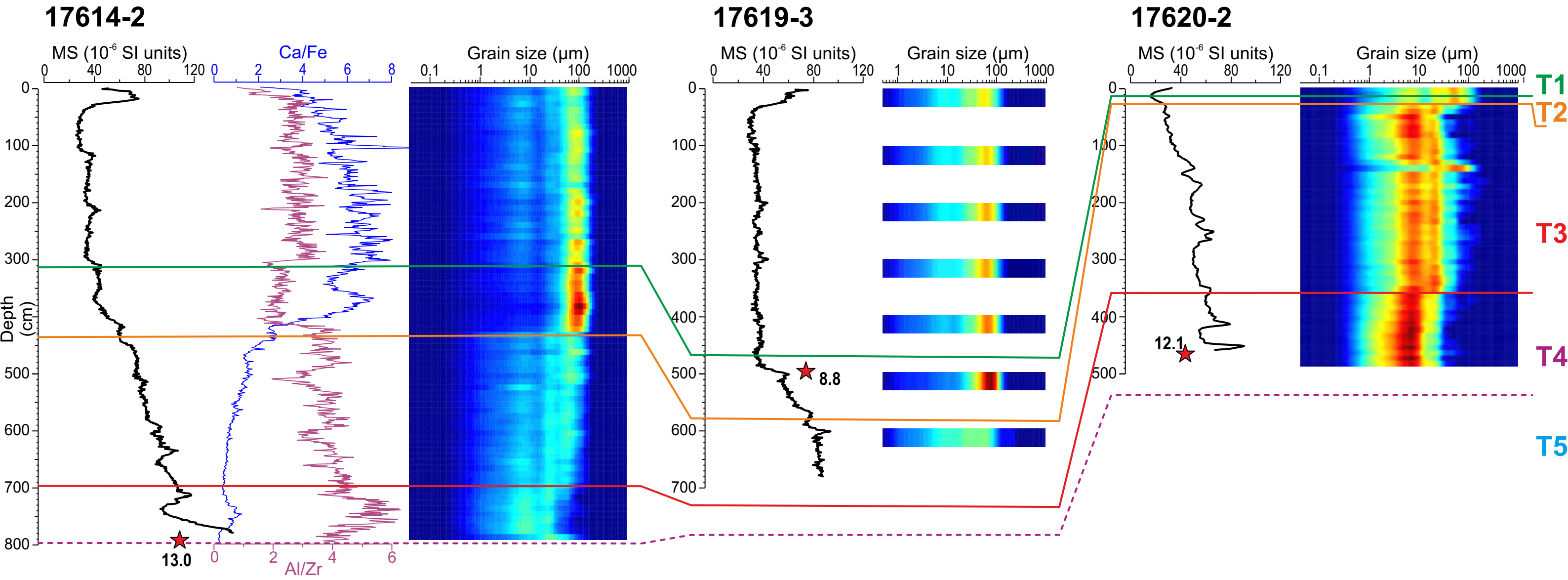
17614-2
MS (10^-6 SI units)
Ca/Fe
Grain size (µm)
Depth (cm)
Al/Zr
13.0
17619-3
MS (10^-6 SI units)
Grain size (µm)
8.8
17620-2
MS (10^-6 SI units)
Grain size (µm)
12.1
T1
T2
T3
T4
T5

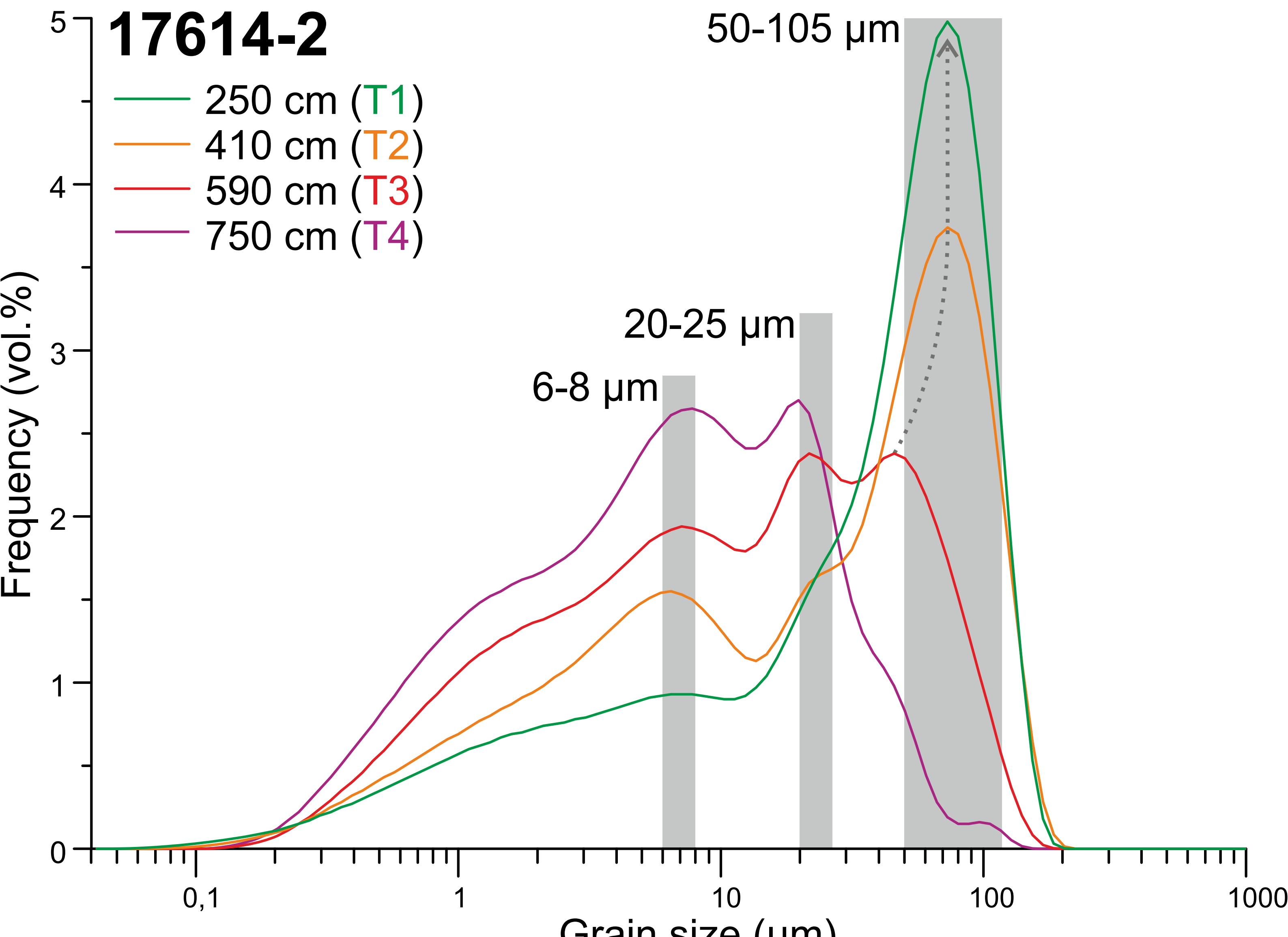

17614-2
250 cm (T1)
410 cm (T2)
590 cm (T3)
750 cm (T4)
50-105 µm
20-25 µm
6-8 µm
Frequency (vol.%)
0
1
2
3
4
5
0,1
1
10
100
1000
Grain size (µm)

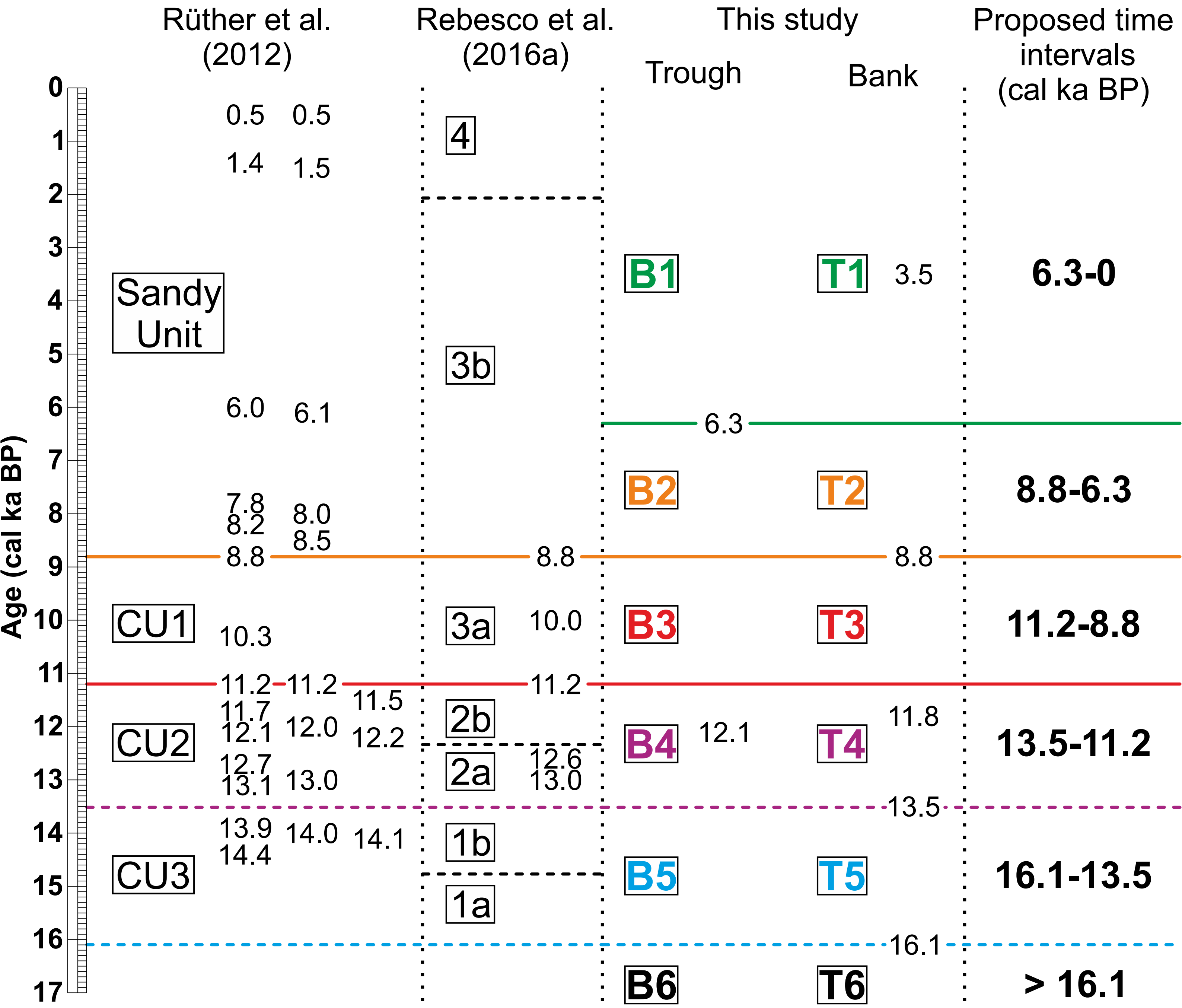

Rüther et al. (2012)
Rebesco et al. (2016a)
This study
Trough
Bank
Proposed time intervals (cal ka BP)
Age (cal ka BP)
0
1
2
3
4
5
6
7
8
9
10
11
12
13
14
15
16
17
0.5
0.5
1.4
1.5
4
Sandy Unit
3b
B1
T1
3.5
6.3-0
6.0
6.1
6.3
B2
T2
8.8-6.3
7.8
8.2
8.0
8.5
8.8
8.8
8.8
CU1
10.3
3a
10.0
B3
T3
11.2-8.8
11.2
11.2
11.2
11.5
11.7
12.1
12.0
12.2
CU2
2b
B4
12.1
T4
11.8
13.5-11.2
12.7
13.1
13.0
2a
12.6
13.0
13.5
13.9
14.4
14.0
14.1
CU3
1b
1a
B5
T5
16.1-13.5
16.1
B6
T6
> 16.1

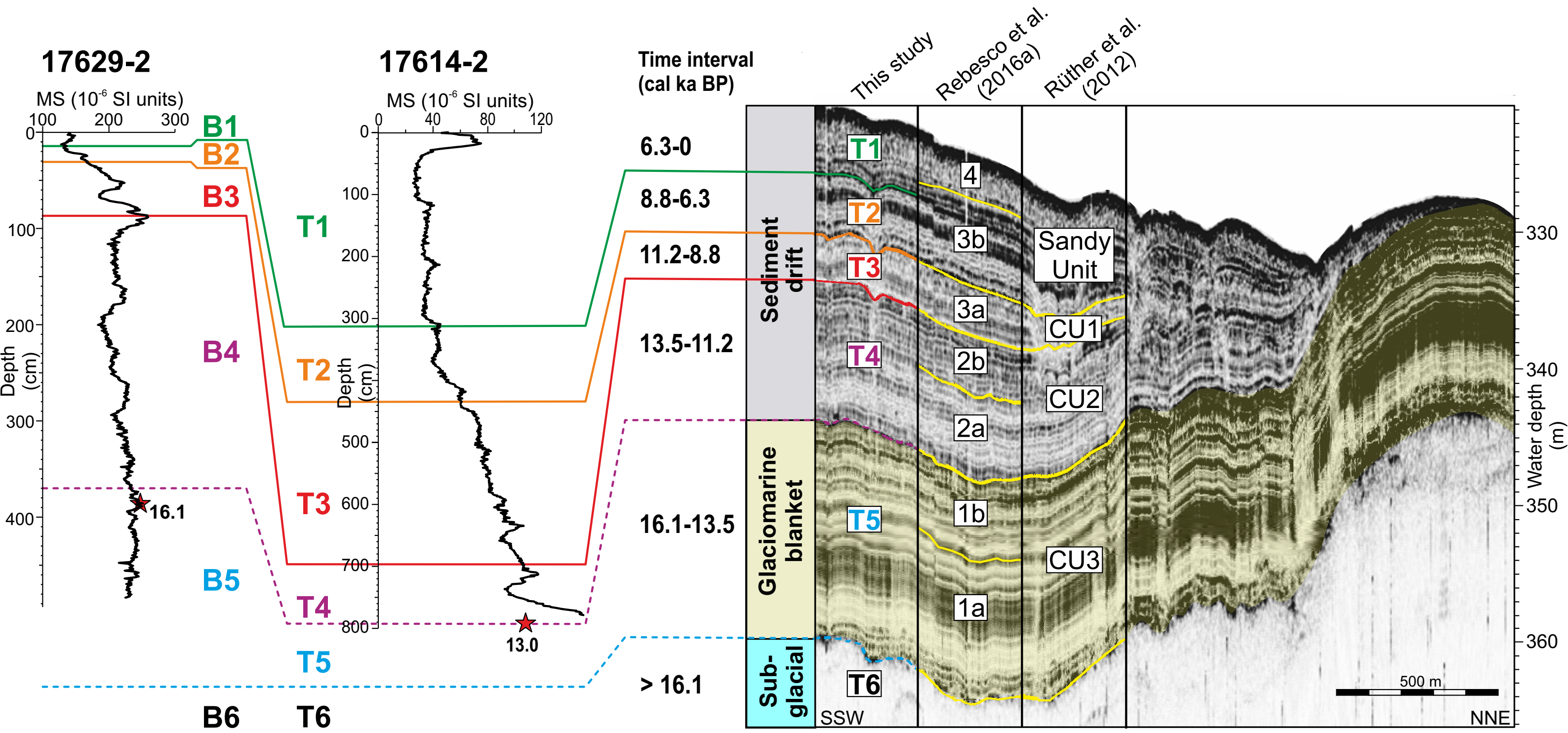

17629-2
MS (10^-6 SI units)
100 200 300
Depth (cm)
0 100 200 300 400
16.1
B1
B2
B3
B4
B5
B6
T1
T2
T3
T4
T5
T6
17614-2
MS (10^-6 SI units)
0 40 80 120
Depth (cm)
0 100 200 300 400 500 600 700 800
13.0
Time interval (cal ka BP)
6.3-0
8.8-6.3
11.2-8.8
13.5-11.2
16.1-13.5
> 16.1
This study
Rebesco et al. (2016a)
Rüther et al. (2012)
Sediment drift
Glaciomarine blanket
Sub-glacial
4
3b
3a
2b
2a
1b
1a
Sandy Unit
CU1
CU2
CU3
SSW
NNE
500 m
Water depth (m)
330 340 350 360

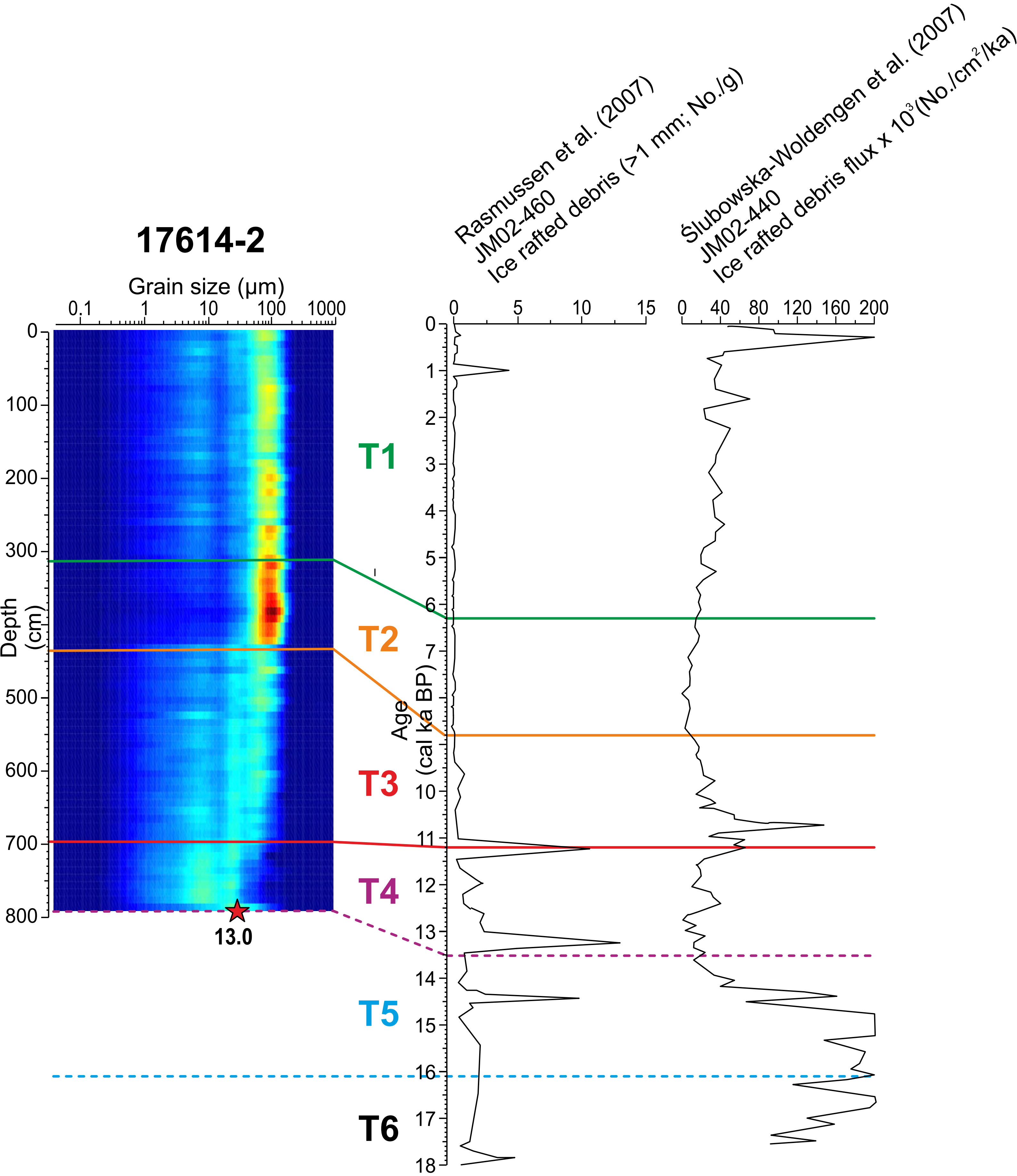

17614-2
Grain size (µm)
0.1
1
10
100
1000
Depth (cm)
0
100
200
300
500
600
700
800
13.0
T1
T2
T3
T4
T5
T6
Age (cal ka BP)
Rasmussen et al. (2007)
JM02-460
Ice rafted debris (>1 mm; No./g)
0
5
10
15
Ślubowska-Woldengen et al. (2007)
JM02-440
Ice rafted debris flux x 10³(No./cm²/ka)
0
40
80
120
160
200

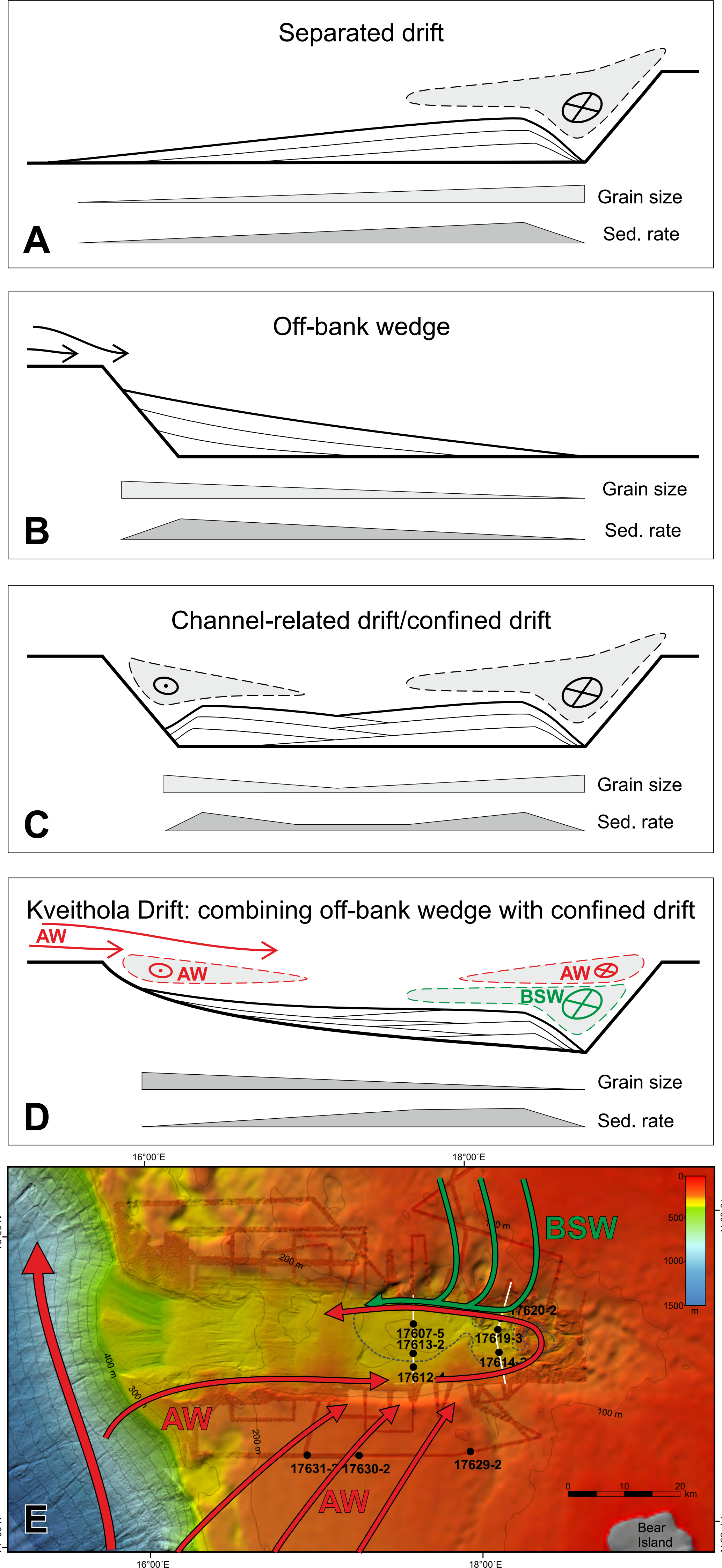

Separated drift
Grain size
Sed. rate
A
Off-bank wedge
Grain size
Sed. rate
B
Channel-related drift/confined drift
Grain size
Sed. rate
C
Kveithola Drift: combining off-bank wedge with confined drift
AW
AW
AW
BSW
Grain size
Sed. rate
D
16°00´E
18°00´E
75°00´N
74°30´N
BSW
200 m
100 m
200 m
400 m
AW
AW
17620-2
17607-5
17613-2
17619-3
17630-2
17629-2
0
500
1000
1500
m
0
10
20
km
Bear Island
E

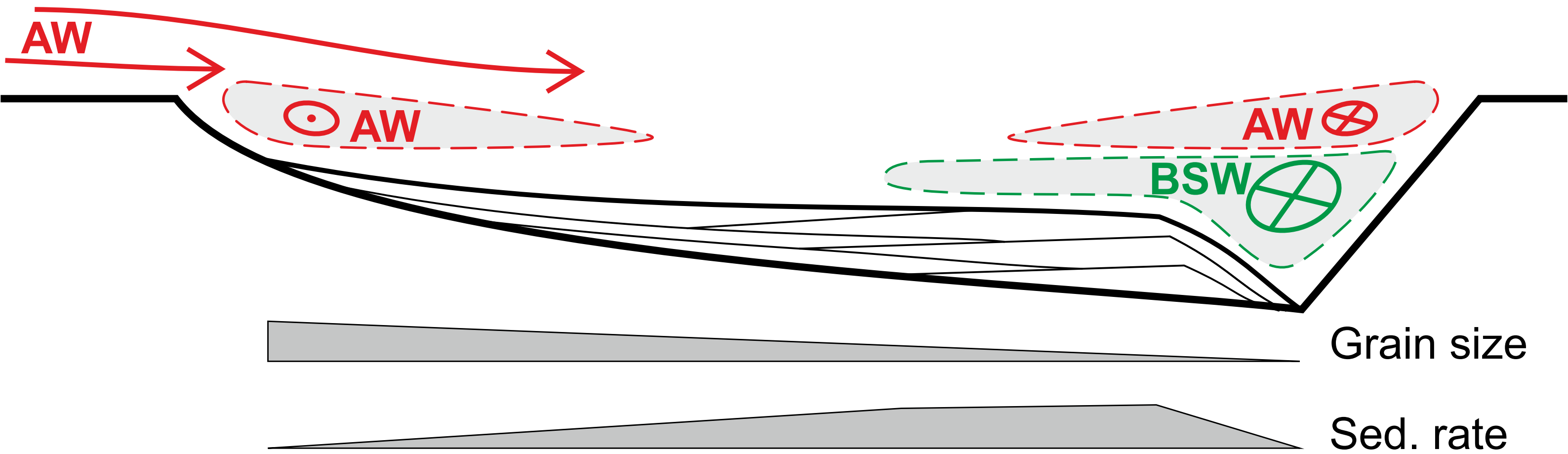

AW = Atlantic Water BSW = brine-enriched shelf waters